Sediment phosphorus composition controls hot spots and hot moments of internal loading in a temperate reservoir

Ellen A. Albright[1,2†] and Grace M. Wilkinson[1,2]

[1]Department of Ecology, Evolution and Organismal Biology, Iowa State University, Ames, IA, USA

[2]Center for Limnology, University of Wisconsin-Madison, Madison, WI, USA

[†] Corresponding Author: ealbright2@wisc.edu

Open research statement

The data (Albright and Wilkinson 2021) and analysis code are available from Zenodo: https://doi.org/10.5281/zenodo.6604143

This manuscript has been accepted for publication at Ecosphere. Once published, the final version of the manuscript will be available via the "Peer-reviewed Publication DOI" link on the right-hand side of this webpage. Please feel free to contact the corresponding author.

Abstract

Phosphorus (P) flux across the sediment-water interface in lakes and reservoirs responds to external perturbations within the context of sediment characteristics. Lentic ecosystems experience profound spatiotemporal heterogeneity in the mechanisms that control sediment P fluxes, likely producing hot spots and hot moments of internal loading. However, spatiotemporal variation in P fluxes remains poorly quantified, particularly in the context of sediment chemistry as a controlling variable. We measured P flux rates and mobile sediment P forms along the longitudinal gradient of a temperate reservoir every two months from February to October of 2020. Both aerobic and anaerobic processes mobilized sediment P throughout the year. High flux rates at littoral sampling sites (8.4 and 9.7 mg P m^{-2} day^{-1}) occurred in late summer under oxic conditions in the overlying water and mobilized labile organic P. High fluxes at the profundal site coincided with hypolimnetic anoxia under ice cover and in mid-summer (11.2 and 17.2 mg P m^{-2} day^{-1}, respectively) and released redox-sensitive P. Several high fluxes substantially skewed the flux rate distribution, providing evidence of hot spots and hot moments of internal loading. We further scaled the measured sediment P flux rates to representative areas of the lakebed to estimate internal P loads at an ecosystem scale. We found that P release from littoral sites under oxic conditions in the overlying water had an outsized impact on total loads. Our findings demonstrate the importance of considering spatial and seasonal variation in sediment P pools and fluxes in order to more accurately estimate internal loads and identify the dominant biogeochemical mechanisms involved.

Key words

Dissolved Oxygen; Phosphorus; Reservoir; Seasonality; Sediments; Spatial Variability.

Introduction

An ecosystem's response to external perturbations results from the interaction of fast- and slow-acting state variables, which fall along a gradient of turnover times from short to long, respectively (Carpenter and Turner 2000). Slow variables determine ecosystem context and control how fast variables respond to external drivers (Walker et al. 2012). Understanding how slow and fast variables interact is necessary for the study and management of complex systems (Crépin 2007; Ward et al. 2019). For example, eutrophication in lakes and reservoirs is often influenced by interacting slow and fast variables at the sediment-water interface. Sediments hold a pool of phosphorus (P), which is the legacy of past external loading and subsequent sedimentation (Søndergaard et al. 2003; Walsh et al. 2019). This P may be retained in the sediments or mobilized and released into the overlying water (i.e., internal P loading; Orihel et al. 2017). Within the sediments there are many different P-containing minerals, organic compounds, and surface complexes, which are vulnerable to different mechanisms of internal loading (North et al. 2015; Orihel et al. 2017). As such, the chemical composition of the sediment P pool is a pivotal slow variable that shapes how the rate of P flux from the sediments (i.e., the fast variable) responds to fluctuations in external drivers (Carpenter 2003).

The response of sediment P flux rates to changing dissolved oxygen availability, the result of external drivers, is shaped by the forms of P present in the sediment. For example, if redox-sensitive P forms (i.e., those associated with iron or manganese oxides) dominate the sediment P pool, then hypolimnetic oxygen depletion will trigger P release due to reductive dissolution of the host minerals (Mortimer 1941; Jensen and Andersen 1992). When water column mixing delivers dissolved oxygen to the sediment surface, oxidized iron and manganese

minerals can stabilize P, which may result in sediment P retention. The idea that oxic conditions prevent P release and that internal loading primarily occurs under anoxia is a persistent paradigm in limnology. However, there is ample evidence that internal P loading occurs under a range of dissolved oxygen conditions based on sediment characteristics (Hupfer and Lewandowski 2008). If sediments hold a large pool of labile organic P, then oxic conditions are expected to mobilize and release P via microbial decomposition and mineralization (Joshi et al. 2015; Horppila et al. 2017). A mixing event that delivers dissolved oxygen to the sediments may also result in sediment resuspension, which releases pore water P and increases diffusive P flux through the sediment profile into the overlying water (Tammeorg et al. 2016). In this example, an influx of dissolved oxygen to the lakebed would stimulate rather than suppress internal loading, especially if the sediments were disturbed. The relationship between dissolved oxygen and P flux is expected to vary with the composition of the sediment P pool, which is heterogenous across the lakebed and over time (Nowlin et al. 2005; Kowalczewska-Madura et al. 2019). However, it is unclear how the interaction between this slow variable and external drivers influences spatiotemporal variability in sediment P fluxes and what the consequences of this variation are at the ecosystem scale.

Lentic ecosystems are highly variable in space and time. Temperate reservoirs are particularly variable due to longitudinal gradients in basin morphometry as well as strong spatial and seasonal variation in thermal mixing, hypolimnetic dissolved oxygen, and organic matter sedimentation (Nowlin et al. 2005; Hayes et al. 2017; Cardoso-Silva et al. 2018). Increasing water depth from riverine to lacustrine regions of a reservoir yields spatial variation in water column mixing and thus chemical conditions at the sediment-water interface (Kimmel and Groeger 1984; Hudson and Vandergucht 2015). Specifically, shallow riverine and transitional

sections remain mixed throughout the open water season, usually maintaining oxygenated conditions above the sediments. Conversely, the deeper lacustrine region will likely experience at least intermittent thermal stratification, which may result in hypolimnetic dissolved oxygen depletion (Hayes et al. 2017). In short, basin morphometry produces spatial variation in the dynamics of external drivers that influence internal P loading. Organic matter sedimentation also varies along the longitudinal gradient and may impact the composition of the sediment P pool. Riverine segments receive more allochthonous organic matter inputs while autochthonous material dominates sedimentation in the lacustrine region (Hayes et al. 2017; Cardoso-Silva et al. 2018). Autochthonous organic matter inputs also vary over space and time due to seasonal algal dynamics and spatial heterogeneity in bloom formation (Buelo et al. 2018; Ortiz and Wilkinson 2021). When combined, spatial and seasonal variation in both redox conditions and the composition of the sediment P pool likely produce hot spots and hot moments of sediment P release.

Hot spots and hot moments are high rates of biogeochemical activity that occur when two reactants are brought together in space and time within an ecosystem (McClain et al. 2003). This biogeochemical phenomenon can be understood within the conceptual framework of fast and slow variables. Specifically, a hot spot-hot moment is the product of an external perturbation delivering a reactant that interacts with the slow variable resulting in a high rate in the fast variable at that moment and location. For example, sudden water column mixing due to a storm delivers dissolved oxygen to the sediment surface, which is rich in labile organic P, resulting in a spike of sediment P release due to aerobic decomposition and mineralization as well as increased diffusive P flux due to sediment disturbance (Tammeorg et al. 2016). This external perturbation interacts with the slow variable (i.e., the sediment P pool) and brings two reactants together (i.e.,

dissolved oxygen and labile organic P), resulting in the hot spot-hot moment of P flux across the sediment-water interface. Hot spots and hot moments disproportionately influence elemental cycles at the ecosystem-scale. For example, temperate waterbodies likely experience hot spots and hot moments of sediment P release such that the majority of the total internal P load may be associated with a few key areas of the lakebed and times throughout the year. As such, efforts to control internal P loading would have the greatest impact by focusing on hot spots and hot moments of P release. However, doing so requires an understanding of the underlying mechanisms. Although hot spots and hot moments have been well-documented, most studies have focused on carbon and nitrogen cycles in streams and riparian soils, and there has been little consideration of both hot spots and hot moments of P cycling, especially in lentic ecosystems (Bernhardt et al. 2017). Additionally, analyses of the mechanisms that produce hot spots and hot moments in biogeochemical cycles remain scarce, undermining our understanding of these extreme events and how they impact ecosystem function. While the environmental conditions that may produce high rates of sediment P flux in lakes and reservoirs have been well-documented, no study to date has explicitly delineated hot spots and hot moments of sediment P release and, more importantly, identified the causal mechanisms of these extreme events.

In order to quantify hot spots and hot moments of sediment P flux and explore the underlying mechanisms, we measured mobile sediment P pools and fluxes over the course of a year and across the lakebed of a temperate reservoir (Figure 1). Specifically, we measured sediment P composition and flux rates at three sites along the longitudinal gradient of the reservoir approximately every other month over the course of 2020, capturing conditions under the ice as well as thermal mixing and stratification events during the open water season. We asked, (Q1) When and where do hot spots and hot moments of sediment P flux rates occur, and

what are the underlying mechanisms? (Q2) How does the slow variable (i.e., the composition of the sediment P pool) change over space and time, and how do these changes relate to P flux rates? (Q3) How do hot spots and hot moments of internal loading scale to the ecosystem level? We hypothesize that there are hot spots and hot moments in the rates of P flux from the sediments that arise from interactions between P speciation and biogeochemical conditions at the sediment-water interface. Over the course of the year, we anticipate that P will be mobilized and released from a variety of sediment P sources. We anticipate that temperature and dissolved oxygen concentrations will be key mechanisms driving internal loading but that the specific effects of these variables will depend on the composition of the sediment P pool. Predicting the occurrence of hot spots and hot moments of internal loading and identifying the causal mechanisms is essential for effectively managing whole-lake P cycling. Our findings demonstrate that the mechanisms driving hot spots and hot moments of internal P loading cannot be understood without capturing both seasonal and spatial variation in fluxes and the composition of the sediment P pool.

Methods

Study site

Green Valley Lake (GVL) is a hypereutrophic reservoir located in southwest Iowa, USA (41°05'58.9"N 94°23'04.7"W, Figure 1), with a discontinuous cold polymictic stratification and mixing pattern. The reservoir lies in the rolling loess prairie region of the western corn belt plains. Row crop agriculture dominates the GVL watershed with 68.4% of the land cover in a corn-soybean rotation. GVL is relatively small (surface area 156.2 ha) and shallow (maximum depth 6.8 m and mean depth 3.2 m), with two main branches meeting at the southern end of the

basin above the dam outflow. As an impoundment of several small tributaries, GVL has a highly irregular shape (shoreline development factor 3.44), characterized by numerous shallow bays and an extensive littoral zone.

We measured spatial variation in sediment P pools and fluxes at three sampling sites distributed along the longitudinal gradient of the west branch of the reservoir. We selected the western branch as this inflow is the main tributary to the reservoir and drains the majority of the watershed. The shallow sampling site (2.5 m) was located near the west inlet, and the water column remained mixed throughout the open water season. The intermediate depth site (4.0 m) was in the middle of the western branch of GVL. Thermal stratification developed under ice and intermittently throughout the open water season. The deep sampling site (maximum water depth 6.8 m) was located at the deepest hole of the reservoir near the dam. Water column stratification and mixing followed the same pattern as the intermediate site (Table 1).

In order to evaluate seasonal patterns in P dynamics, we sampled these sites throughout 2020 on day of year (DOY) 39, 117, 181, 223, and 298 (winter, spring, mid-summer, late summer, and autumn, respectively). The timing of the sampling events was designed to capture ice cover, thermal stratification in spring, and mixing events in the summer and autumn (Table 1). The shallow site was not sampled in February due to unsafe ice conditions created by a congregation of Canada geese (*Branta canadensis*). The sampling event in late summer occurred immediately following a derecho, an intense windstorm affecting a large geographic area (Corfidi et al. 2016; Goff et al. 2021). Although GVL lay at the edge of the derecho's path, windspeeds at the reservoir are estimated to have exceeded 65 kph, fully mixing the water column at all sites (Table 1).

Vertical profiles and water chemistry

To monitor thermal mixing patterns in GVL, we deployed vertical strings of temperature sensors at the shallow and deep sites (HOBO 8K Pendant Temperature Data Logger). Sensors were placed every 0.5 m up to 3 m deep and then every 1 m to the lakebed. The sensors logged water temperature every 30 minutes from spring to late summer. At each sampling site and event, we also measured water column profiles of temperature and dissolved oxygen using a YSI ProDSS Multiparameter Digital Water Quality Meter. Additionally, we collected water samples 0.25 m below the water surface and 0.5 m above the sediment-water interface for analysis of total P (TP), soluble reactive P (SRP), total nitrogen, nitrate, and suspended solids (see Appendix S1 for full methods and data). Subsamples were filtered in the lab (0.45µm GF/C filters) for SRP analysis, and all samples were preserved with concentrated sulfuric acid to pH 2. TP samples underwent persulfate digestion prior to analysis (Standard Methods 4500-P B.5). We measured SRP and TP concentrations with the molybdenum blue method modified from Murphy and Riley (1962; Standard Methods 4500-P E) using a SEAL Analytical AQ2 Discrete Analyzer.

Sediment P fluxes

To quantify sediment P fluxes, we collected intact sediment cores and incubated them under ambient conditions in the lab while measuring P exchange with the overlying water. For each sampling site and event, three replicate sediment cores were collected using a gravity corer (inner diameter 5 cm, length 50 cm), such that there were approximately 25 cm of sediment and 25 cm of overlying water. The sediment cores and the overlying water were sealed in clear, acrylic core sleeves and transported at 4°C. In the laboratory, we exposed cores to temperature and dissolved oxygen treatments corresponding to ambient conditions at each site (Appendix S1

Table S1, Figure S1). Temperature treatments were achieved by securing the cores in either a water bath or an incubation chamber. Dissolved oxygen levels were manipulated by bubbling either air mixtures or N_2 through the overlying water. A slow, consistent bubble rate was used to gently mix the water column without disturbing the sediment surface. After the cores were placed in the incubation system, we measured the height of the water column within each core tube to calculate the water volume.

Samples of the overlying water were collected 12, 36, 60, and 84 hours after the initial incubation set-up. For each daily sampling, 50 mL of water was removed for analysis of TP. An equivalent volume of hypolimnetic water, collected from 0.5 m above the sediment surface at the corresponding site, was used to replace the volume removed. The replacement hypolimnetic water was also analyzed for TP daily to account for changes in water column P due to sampling and water replacement. Samples were preserved with concentrated sulfuric acid to pH 2 and stored at 4°C before undergoing persulfate digestion and analysis for TP (Standard Methods 4500-P B.5, E). We monitored water temperature, dissolved oxygen, and pH (YSI ProDSS Multiparameter Digital Water Quality Meter) daily to ensure that the overlying water remained representative of ambient conditions in the reservoir at the time of sampling.

The change in TP in the overlying water was used to calculate daily, areal P flux rates for each core. We determined flux rates based on TP in order to capture all forms of P that may be exchanged between sediments and the overlying water including phosphate, dissolved organic P forms, and particulate P. We first calculated the mass of P in the overlying water immediately following the collection of the daily water sample as well as the mass of P in the replacement water. We then determined how the addition of the replacement water changed the TP concentration of the overlying water. The daily change in TP concentration was calculated as the

difference between this new TP concentration after the addition of replacement water and the TP concentration measured in the water column the next day (see Appendix S1, Equations S1-S4). The P flux rate was then calculated as:

$$\text{P flux rate (mg P m}^{-2}\text{ day}^{-1}) = (C_t - C_0) * V / A / d \quad \text{(Eq. 1)}$$

Where C_t is the water column TP concentration (mg L^{-1}) on a given day, C_0 is the TP concentration (mg L^{-1}) from the previous day after the addition of replacement water, V is the total volume (L) of water overlying the sediment core, A is the area (m^2) of the sediment surface, and d is the number of days between measurements (Ogdahl et al. 2014). Over a 4-day incubation, we calculated three daily P flux rates for each sediment core. We took the mean of these temporal replicates to yield one P flux rate per core, per incubation. Mean flux rate and standard error of the mean for the three replicate sediment cores from each sampling site and event were then used to estimate P flux rate through time at the various sites.

Sediment P content and composition

At each sampling site and event, we collected an additional sediment core for analysis of sediment P composition, total P content, and physical characteristics (see Appendix S1 for sediment physical characteristics methods, Equations S5-S7). We extruded the first 10 cm of the sediment profile into an acrylic core sleeve, which was sealed immediately to maintain ambient redox conditions. The top 10 cm of sediment is considered actively exchanging with the overlying water as diffusive processes and turbulent disturbance can occur in sediments this deep (Forsberg 1989). This surface sediment layer also holds P forms that are likely to be transformed or released on relatively short timescales (Orihel et al. 2017). Samples were transported and stored at 4°C until analysis, which began within 18 to 36 hours of sample collection. Sediments

were handled under N_2-atmosphere in a glove bag and thoroughly homogenized before removing three replicate subsamples from each core. The replicates were analyzed for three mobile P species (loosely-bound, redox-sensitive, and labile organic P) as well as a more stable P fraction (aluminum-bound P) via sequential extraction following Lukkari et al. (2007). Dried sediments were used to quantify total P.

To begin the sequential P extractions, subsamples of fresh sediment equivalent to 0.5 g of dry sediment were weighed into polyethylene centrifuge tubes. This same sediment pellet was used throughout the sequential extraction procedure. All extractions were performed on an orbital shaker table at 25°C. Extractant and rinse solution volumes (50 mL), shaker table speed (200 rpm), and centrifuge time and speed (30 minutes at 3000 rpm) were consistent across all extractions. In general, each extraction involved shaking the sediment pellet in the extraction solution, centrifuging, and pouring off the supernatant. All extractions included at least one rinse, in which the sediment pellet would shake for 15 minutes in a rinse solution to minimize tailing. The supernatant of the rinse extractions was combined with the primary extraction supernatant. Following each extraction, the total supernatant was preserved with concentrated sulfuric acid to pH 2 to keep metals soluble and achieve the required pH for color development during SRP and TP analyses. All SRP and TP concentrations were corrected for the extractant volume and the mass of sediment used to determine the P concentration per gram of dry sediment (See Appendix S1, Equations S8-S13).

Loosely-sorbed and pore water P were extracted in 0.46 M N_2-purged sodium chloride (NaCl) for one hour. One rinse in 0.46 M N_2-purged NaCl was used, and the combined extract solution was preserved for TP analysis (Standard Methods 4500-P B.5, E). Redox-sensitive P species were extracted in a 0.11 M bicarbonate – 0.1 M sodium dithionate (BD) solution for one

hour. This extraction included two rinses with BD solution and one NaCl rinse. The combined extract supernatant was bubbled with compressed air for at least 90 minutes to remove dithionite before being preserved for TP analysis. Labile organic P and P associated with aluminum oxides were determined with an 18-hour extraction in 0.1 M sodium hydroxide (NaOH). One NaOH rinse was used, followed by one NaCl rinse. The combined extract supernatant was analyzed in two portions. First, a portion was filtered (0.45µm GF/C filters) and analyzed for SRP (Standard Methods 4500-P E). This SRP concentration was used to calculate the sediment concentration of aluminum-bound P. The remaining supernatant was digested and analyzed for TP. The labile organic P fraction was determined as the difference between the total NaOH-extractable P and the aluminum-bound P. Total sediment P concentrations were measured following a hot acid digestion on dried, ground, and homogenized sediments. Three replicate subsamples (0.2 g) of the dried sediment were combusted it at 550°C for 2 hours and then boiled on a digestion block in 50 mL of 1 M HCl for 2 hours at 150°C. Following digestion, samples were diluted to 50 mL with deionized water, and adjusted to pH 2 using 0.1 M NaOH before TP analysis.

Statistical analyses

As there is no universal, quantitative method for delineating hot spots and hot moments of biogeochemical fluxes in a distribution of flux measurements (Bernhardt et al. 2017), we used a variety of approaches to explore the distribution of P flux rates and determine whether the observed spatiotemporal variation indicated hot spots or hot moments. We first identified statistical outliers in the distribution, defined as flux measurements falling above or below 1.5 times the interquartile range. We further quantified the shape of the P flux distribution by calculating skewness (m_3; Appendix S1, Equation S14), which identifies whether the distribution

292 is symmetric ($m_3 < 0.5$) or if extreme flux rates, presumably due to hot spots or moments, skew
293 the distribution ($m_3 > 0.5$). We further evaluated the influence of high flux rates on the
294 distribution by iteratively removing the highest flux rates and recalculating skewness. Through
295 this process, we determined how many of the highest flux rates would need to be removed to
296 produce a nearly symmetric distribution (Gakuruh 2017).

297 In order to evaluate how the composition of the sediment P pool varied across sites and
298 seasons, we performed a compositional data analysis. Compositional data analysis tests for a
299 difference of proportions among multivariate observations, allowing us to test differences in the
300 relative abundance of P fractions across different sites and events (Filzmoser et al. 2018). The
301 compositional analysis was defined by the concentrations of loosely-bound (porewater and
302 surface sorbed), redox-sensitive (Fe- and Mn-bound), aluminum-bound, and labile organic P.
303 The sediment P concentrations were center logratio transformed prior to a principal components
304 analysis (PCA) on the covariance matrix, as not to bias the analysis to the most abundant
305 sediment P fractions.

306 To estimate the total sediment P load (kg day^{-1}) in the reservoir for each sampling event,
307 we multiplied the mean P flux rate (mg m^{-2} day^{-1}) at each sampling site by the lakebed area (m^{-2})
308 within representative depth contours corresponding to each site. The shallow site measurements
309 were assigned to the 1.2 – 3.6 m depth contour, the intermediate depth site measurements were
310 assigned the 3.6 – 5.6 m depth contour, and the deep site measurements were assigned the 5.6 –
311 6.8 m depth contour. The threshold of 5.6 m was determined based on the historical mean depth
312 of hypoxia in the water column. We excluded areas shallower than 1.2 m, including the sediment
313 retention basins north of the reservoir, because these areas are mainly in secluded, wind-
314 protected bays (Figure 1). Our sampling sites, which were centrally located along a branch of the

reservoir, cannot reasonably be extrapolated to these shallow areas due to expected differences in wave disturbance and the depositional environment (Kleeberg et al. 2013). To calculate the lakebed area within the representative depth contours, we used the length of each depth contour from a bathymetric map produced by the Iowa Department of Natural Resources. The area between depth contours is a trapezoid-shaped area of lakebed wrapping around the reservoir basin. We calculated this area as:

$$A = \left(\frac{length\ 1 + length\ 2}{2}\right) \times h \quad \text{(Eq. 2)}$$

Where length 1 and 2 are the lengths of the bounding depth contours, and *h* is the assumed average distance between the depth contours across the lakebed, estimated using the Pythagorean theorem:

$$h = \sqrt{(depth\ 2 - depth\ 1)^2 + \left(\sqrt{area\ 1} - \sqrt{area\ 2}\right)^2} \quad \text{(Eq. 3)}$$

Where depth 1 and 2 refer to the water depth of the top and bottom depth contours, and area 1 and 2 represent the planar areas at the top and bottom depth contours. This method assumes that the lakebed follows a linear slope between the bounding depth contours, so it is likely an underestimate of the true area of the sediment surface. After determining the lakebed area corresponding to each sampling site, we multiplied this area by the flux rates and then summed across all three load estimates for the total load for that sampling event. To propagate the uncertainty of this estimate, we added the standard error of the mean values in quadrature.

All data are available in Albright and Wilkinson (2021), and analysis code is available from Zenodo: https://doi.org/10.5281/zenodo.6604143. All analyses were completed in R version 3.6.0 (R Core Team 2019) using the sf (Pebesma 2018), spData (Bivand et al. 2021), fGarch (Wuertz et al. 2020), robCompositions (Filzmoser et al. 2018), and vegan packages (Oksanen et al. 2019).

Results

Physiochemical conditions

Water column chemistry and thermal structure varied across sampling sites and over the course of the year (Table 1). At the shallow site, the water column remained mixed throughout the open water season and the sediment-water interface remained oxic (dissolved oxygen range 5.4-10.2 mg L^{-1}). At the intermediate and deep sites, thermal stratification first developed after ice-off. Intermittent stratification continued through late summer, after which the water column was mixed at both sites. The sediment-water interface at the intermediate depth site remained oxic throughout the study period (dissolved oxygen range 4.8-12.6 mg L^{-1}), but the deep site experienced periodic hypoxia (dissolved oxygen range 0.3-8.7 mg L^{-1}). On the day of the late summer sampling (DOY 223), a derecho passed over the reservoir, prompting a mixing event, as evidenced by an isothermal water column at all sampling sites. Following the derecho, the relative contribution of inorganic solids to the total suspended solids pool was much greater than any other point throughout the year in both surface and bottom waters, suggesting that the storm resulted in sediment disturbance and a well-mixed water column (Appendix S1 Table S2).

Hypolimnetic P concentrations followed a similar seasonal pattern across sampling sites (Figure 2). At the deep and intermediate sites, hypolimnetic TP concentrations remained stable between under-ice sampling (DOY 39) and early spring (DOY 117). Hypolimnetic concentrations of both TP and SRP then increased from spring through late summer, peaking at 318.0 to 370.9 µg L^{-1} and 116.3 to 168.5 µg L^{-1}, respectively, before declining in autumn. Although these nutrient concentrations are quite high, the dynamics of P in the water column in

2020 are consistent with concentrations and seasonal patterns previously measured in GVL (Appendix S1 Figure S2).

Sediment P fluxes

Sediment P flux rates varied substantially among sampling sites and across seasons (Figure 2, Appendix S1 Table S3). Flux rates were most variable over time at the deep site; however, these profundal sediments consistently released P to the overlying water from winter to mid-summer (DOY 39, 117, 181), and then had moderate retention or release rates in the late summer and autumn (DOY 223, 298). Sediments from the intermediate depth site retained P under ice cover (DOY 39), but released P in spring and late summer (DOY 117, 223). The shallow site followed a similar seasonal pattern with sediment P release in spring and late summer (DOY 117, 223) and negligible fluxes in mid-summer and autumn (DOY 181, 298). Overall, the highest rates of P release occurred at the shallow and intermediate sites in late summer (DOY 223) and in winter and mid-summer (DOY 39, 181) at the deep site.

Over the course of the year, sediment P release occurred under a broad range of dissolved oxygen concentrations at the sediment-water interface (Figure 3, Table 1). At the deep site, nearly anoxic conditions were associated with elevated rates of P release in winter and mid-summer (DOY 39, 181; dissolved oxygen 1.1 and 0.3 mg L^{-1}, respectively). However, most of the observed instances of P release occurred when oxygen was available at the sediment-water interface. For example, sediments across all three sampling sites released P under oxic conditions in spring (DOY 117; dissolved oxygen range 5.8-9.4 mg L^{-1}), and high rates of oxic P release occurred at the intermediate and shallow sites in late summer (DOY 223; dissolved oxygen 4.8 and 7.2 mg L^{-1}, respectively). The effect of dissolved oxygen availability on sediment P flux

rates differed between the deep site and more shallow sampling sites, and elevated P release rates were observed under both oxic and anoxic conditions.

The shape of the distribution of sediment P flux rates over the course of 2020 provides evidence of hot spots and hot moments of sediment P release in GVL. The distribution of P flux rates was centered near 0 mg P m^{-2} day^{-1} with the majority of the rates falling between -10 and 10 mg P m^{-2} day^{-1} (Appendix S1 Figure S3). The first statistical moment, or mean, of the distribution was 3.4 mg P m^{-2} day^{-1}. The distribution was moderately positively-skewed (third standardized statistical moment $m_3 = 0.818$) due to five high release rates (range 16.2-23.6 mg P m^{-2} day^{-1}). The four highest of these points were classified as statistical outliers. The high release rates were from the deep sampling site in winter and mid-summer (DOY 39, 181) as well as fluxes in late summer (DOY 223) from the intermediate and shallow sites (Appendix S1 Figure S4). Subsampling the dataset to exclude the five highest flux rates resulted in an approximately symmetric distribution ($m_3 = 0.462$; Appendix S1 Table S4). The mean flux rate with the five highest rates excluded was 1.2 mg P m^{-2} day^{-1}, which is almost a third of the mean flux rate for the whole distribution. The presence of high flux rates that skew the distribution indicate hot spots and hot moments of sediment P release.

Sediment P composition

To understand spatiotemporal variation in sediment P fluxes, we also measured changes in the sediment P pool, the slow variable, across seasons and sampling sites. The total sediment P pool varied among sites and seasons. Following expected patterns in sediment focusing, total P concentrations increased along the longitudinal gradient of the reservoir and were far greater at the deep site than the intermediate and shallow sites (Figure 4A). At the deep site, sediment total

406 P increased slightly from winter to spring (DOY 39-117), decreased between spring and mid-
407 summer (DOY 117-181), and then increased through autumn (DOY 298). At the intermediate
408 side, total P also increased from winter to spring (DOY 39-117), but then decreased through late
409 summer (DOY 223) before increasing in autumn (DOY 298). Sediment total P decreased
410 gradually from spring to autumn at the shallow site, except for a slight increase between mid-
411 and late summer (DOY 181-223; Appendix S1 Figure S5).

412 Across all sampling sites, redox-sensitive P was the dominant pool of mobile P found in
413 the reservoir sediments constituting an average of 40.9-51.3 percent of the total P pool across
414 sites (Figure 4A). The concentrations of all measured sediment P species were dynamic over
415 time across the reservoir. Redox-sensitive P concentrations decreased over the course of the year
416 at the shallow site. At the intermediate depth site, redox-sensitive P concentrations increased
417 from winter to spring (DOY 39-117), declined through late summer (DOY 223), and increased
418 until autumn (DOY 298). Redox-sensitive P at the deep site declined from winter through late
419 summer (DOY 39-223), before increasing through autumn (DOY 223-298; Figure 4B).

420 Overall, concentrations of labile organic P increased from spring to autumn at all study
421 sites, except for slight declines between mid-summer and late summer (DOY 181-223) at the
422 intermediate and shallow sites (Figure 4C). Aluminum-bound P concentrations declined from
423 spring through autumn at the shallow site. At the intermediate depth site, concentrations
424 increased from winter to spring (DOY 39-117), declined through late summer (DOY 223), and
425 then increased again. At the deep site, aluminum-bound P followed an inverse pattern to that of
426 redox-sensitive P, increasing from winter through late summer (DOY 39-223) and decreasing
427 from late summer to autumn (DOY 223-298; Figure 4D). Temporal patterns in loosely-bound P
428 varied across sites with declines over the study period at the shallow site, a gradual increase over

time at the intermediate site, and steady concentrations at the deep site except for an increase from late summer to autumn (DOY 223-298; Figure 4E).

We used PCA as part of a compositional data analysis to explore spatiotemporal variation in overall sediment P composition. The compositional analysis was defined by the concentrations of loosely-bound, redox-sensitive, aluminum-bound, and labile organic P (Figure 5). The first principal component (PC1) explained 76.77% of the variation in the dataset and was highly correlated with loosely-bound and redox-sensitive P content. The second principal component (PC2) explained (14.35%) of the variation and was more closely associated with labile organic P content. The first two principal components explained 91.12% of the variance in the dataset. Overall, sediment samples from the shallow site had lower loosely-bound and redox-sensitive P content, whereas these species were more prevalent in the deep site sediments. The composition of the sediments from the intermediate site fell between that of the deep and shallow sites. Over the course of the study period, sediment composition from all study sites generally decreased in loosely-bound and redox-sensitive P content and increased in labile organic P content.

Sediment physical characteristics remained relatively stable over time but varied along the longitudinal gradient of the reservoir (Appendix S1 Table S5). Loss on ignition organic matter content was greatest at the deep site (13.08 ± 0.98 %) and similar between the shallow and intermediate sites (8.83 ± 0.75 and 8.54 ± 0.71 %, respectively). Water content was also highest at the deep site (86.18 ± 0.49 %) and comparable between the shallow and intermediate sites (71.83 ± 0.75 and 75.72 ± 3.0 %, respectively). Bulk density decreased from the shallow (1.19 ± 0.006 g cm^{-3}), to intermediate (1.16 ± 0.024 g cm^{-3}), to deep site (1.07 ± 0.003 g cm^{-3}).

Total P load

We estimated daily sediment P loads for each sampling event by scaling the measured flux rates to representative areas of the lakebed to better understand the ecosystem-scale consequences of the P fluxes. The estimated total P load across the lakebed varied over time, with higher loads occurring under oxic conditions in spring and late summer (DOY 117, 223; Figure 6; Appendix S1, Table S6). The greatest total P load occurred in late summer (DOY 223) due to high flux rates from the shallow and intermediate sites under oxic conditions in the overlying water (Figure 3). Oxic conditions were also associated with high total P loads in spring (DOY 117), when low P release rates across all sampling sites resulted in a substantial total P load due to the large area of the lakebed releasing P. In contrast, high rates of sediment P release under anoxic conditions at the deep site in winter and mid-summer (DOY 39, 181) did not translate into a high total P load due to the small area of lakebed involved. The greatest P loads were associated with aerobic sediment P release across a broad area of the lakebed. The seasonal trend in the estimated total P load mirrors the observed time series for hypolimnetic TP and SRP (Figure 2).

Discussion

Hot spots and hot moments of sediment P flux rates

There was clear evidence of hot spots and hot moments of sediment P release in the study reservoir over the course of 2020. These elevated rates of sediment P flux occurred in late summer at the shallow and intermediate depth sites as well as in winter and mid-summer at the deep site. While the highest rates of sediment P release occurred under anoxic conditions at the deep site, the other elevated flux rates at the shallow and intermediate sites happened when dissolved oxygen was available at the sediment-water interface. Other studies of hypereutrophic reservoirs have also observed aerobic sediment P release, which was associated with intense

476 algal production and P mobilization during decomposition of sediment organic matter (Song and
477 Burgin 2017; McCarty 2019). As a hypereutrophic waterbody, GVL also experiences severe
478 algal blooms throughout the summer months, so it is likely that microbial decomposition of algal
479 detritus contributed to the observed aerobic P release.

480 However, sediment P release when the overlying water is oxic is very complex and may
481 involve both aerobic and anaerobic processes in the sediment profile. The depth of dissolved
482 oxygen penetration into the sediments is typically very shallow such that much of the sediment
483 profile remains anoxic (Hupfer and Lewandowski 2008). Therefore, P mobilization via aerobic
484 decomposition and subsequent mineralization is limited to a thin, surficial layer of sediment.
485 Anaerobic processes of P mobilization, such as the reductive dissolution of redox-sensitive P
486 minerals, can still occur deeper within the sediment profile. The P mobilized via anaerobic
487 processes will diffuse upward and may be released into the overlying water. The P sorption
488 capacity of the sediments and the availability of alternative electron acceptors will influence
489 whether mobilized P will diffuse into the overlying water or remain in the sediments (Caraco et
490 al. 1993). The observed P release under oxic conditions at the shallow and intermediate depth
491 sites likely represents P mobilized via aerobic decomposition of sediment organic matter as well
492 as anaerobic processes within the sediment profile.

493 A severe storm disturbance on the late summer sampling date could have further
494 exacerbated internal loading at the shallow and intermediate sites. The late summer sampling
495 event occurred immediately following a derecho, which mixed the reservoir water column and
496 disturbed sediments. Sediment resuspension has been shown to increase diffusive P flux from
497 sediments into the overlying water, even after the sediments have settled following the
498 disturbance (Tammeorg et al. 2016). Resuspension dilutes the pore water near the sediment

surface, prompting diffusion of soluble P from deeper within the sediment profile and thus enhancing diffusive P fluxes into the water column (Tammeorg et al. 2020). It is likely that the high rates of aerobic P release observed at the shallow and intermediate sites in late summer resulted from both P mineralization from organic matter and sediment disturbance brought on by the storm event. Bottom water TP and SRP concentrations also peaked at this time, indicating that these high flux rates influenced whole-reservoir P dynamics.

The highest rates of P flux from the deep site occurred under ice cover and in mid-summer under nearly anoxic conditions at the sediment-water interface. Profundal sediment P release during summer anoxia has been recorded in many other waterbodies and attributed to reductive dissolution of redox-sensitive P minerals (Mortimer 1941; Nowlin et al. 2005; Kowalczewka-Madura et al. 2019). However, winter measurements of sediment P fluxes are uncommon (Cavaliere and Baulch 2020). Of those measurements that have been made under ice, many studies report low flux rates (Orihel et al. 2017), while others have measured substantial winter loading (Reedyk et al. 2001; North et al. 2015). Our results provide further evidence that mobilization and release of sediment P is still possible under ice cover. Despite the high flux rates measured under ice, hypolimnetic TP concentrations did not increase from winter to the next sampling event in spring. The winter P fluxes may not have been sustained long enough to cause a noticeable increase in water column P. Alternatively, the P released under ice-cover could have been exported downstream before the spring sampling event or diluted during ice melt (Cavaliere and Baulch 2020). The relative importance of winter internal loading is likely system-specific, but to assume that winter P fluxes are negligible risks biasing estimates of annual internal loading.

Sediment core incubations are a common tool for measuring sediment P flux rates (Orihel et al. 2017); however, the approach also has limitations (Oghdal et al. 2014). The main assumption when using core incubations to quantify sediment flux dynamics is that the conditions in the core are representative of the conditions in the waterbody. In an effort to meet this assumption, we incubated cores at ambient temperature and oxygen conditions at the time of collection, monitoring the temperature, dissolved oxygen, and pH daily in the cores. Overall, the experimental set-up mimicked ambient conditions (Appendix S1 Table S1, Figure S1). We also used measurements from replicate cores and multiple days of incubation to estimate daily mean flux rates at a site for a given sampling event in order to capture small-scale spatiotemporal variability in the estimate while comparing across larger spatial and temporal scales. Additionally, we limited our incubations to 3.5 days in order to minimize artifacts that can occur in long-term incubations such as the depletion of organic matter or other key nutrients. Finally, we compared our core incubation-based flux measurements to TP dynamics in the reservoir as another way to verify that the qualitative patterns we observed in flux rates matched the changes in TP concentration measured in the reservoir. These strategies combined provide confidence that the broad-scale spatiotemporal patterns in sediment P flux that we measured reflect the dynamics occurring across sites and seasons in the ecosystem.

Sediment P composition controls flux response to dissolved oxygen

Over the course of the year, we measured internal P loading under a wide range of dissolved oxygen concentrations at the sediment-water interface. Although the dominance of aerobic versus anaerobic internal loading shifted over sites and seasons, both processes were important pathways for P recycling between sediments and the overlying water. In order to

understand why sediment P fluxes responded differently to dissolved oxygen conditions across space and time, we measured the chemical composition of the sediment P pool. We hypothesized that this slow variable shapes how fluxes respond to external drivers that alter dissolved oxygen availability. Spatiotemporal variation in sediment P composition corresponded to variation in sediment P flux rates. Specifically, instances of P release under oxic conditions mainly coincided with declines in labile organic P. Sediment P release during hypolimnetic anoxia and the deep site corresponded to decreasing redox-sensitive P concentrations in the sediments.

A change in the concentration of a sediment P fraction over time could indicate flux across the sediment-water interface or a transformation within the sediments. Evaluating temporal change in both total sediment P and various P fractions helps to distinguish between these processes. At the deep site of the reservoir, change in total and redox-sensitive P concentrations mirrored P flux rates over time. Redox-sensitive P declined steadily from winter to mid-summer, and then sharply decreased (35% decrease) from mid- to late summer. The mid-summer sampling event was a hot spot-hot moment of P release from the profundal sediments that coincided with hypolimnetic anoxia at the deep site. The decline in redox-sensitive P from spring to late summer suggests that the high flux rates in mid-summer were the result of reductive dissolution of redox-sensitive P minerals under anoxic conditions. However, total P only declined from spring to mid-summer, suggesting that some of the redox-sensitive P mobilized between mid- to late summer remained in the sediments. The concentration of aluminum-bound P at the deep site followed the inverse pattern of redox-sensitive P. This temporal pattern suggests that a portion of the P mobilized from redox-sensitive minerals may have sorbed to available aluminum oxides rather than being released into the overlying water.

Concentrations of labile organic P in the sediments generally increased over the course of the year at all sampling sites, likely due to organic matter sedimentation. However, declines were measured at the shallow and intermediate sites from mid- to late summer, indicating that the elevated rates of aerobic P release measured at these sites in late summer involved P mineralization following decomposition of labile organic materials. Sediment total P generally decreased during this time as well, specifically from spring to late summer at the intermediate site and from spring to autumn at the shallow site. The decline in total P at these sites extends beyond the short period of decreasing labile organic P concentrations and is likely driven by declines in redox-sensitive P at these sites over the same time. Temporal coherence between sediment P release and declines in sediment total, labile organic, and redox-sensitive P underscores the complexity of P mobilization under oxic conditions and the variety of P species that may be released.

Our hypothesis that there are hot spots and hot moments of internal loading resulting from interactions between sediment P composition and biogeochemical conditions at the sediment-water interface was supported in our study reservoir. We found that anoxic conditions can trigger the rapid mobilization and release of P from redox-sensitive P pools regardless of water temperature. We also measured P release originating from labile organic materials as well as redox-sensitive minerals under aerobic conditions and found that these fluxes were enhanced following a storm disturbance. Our findings underscore the importance of considering both aerobic and anaerobic pathways of internal loading, especially in productive waterbodies. Our work supports the idea of a "perpetual cycle of internal P loading" in hypereutrophic waterbodies, as proposed by Song and Burgin (2017). The perpetual cycle describes a positive feedback loop that develops as lakes become increasingly eutrophic. Increased algal production

589 enhances inputs of detritus to the sediments, producing a large pool of sediment labile organic P
590 that is susceptible to aerobic release (Baines and Pace 1994; Frost et al. 2019). Sediment P
591 release may then occur under both anoxic and oxic conditions. High internal P loads sustain
592 frequent algal blooms, the detritus of which further fuels aerobic sediment P release via
593 decomposition and mineralization. This positive feedback loop likely introduces hysteresis to
594 maintain waterbodies in a hypereutrophic state. Clear evidence of sediment P release under both
595 oxic and anoxic conditions in GVL indicates that the reservoir has entered this proposed cycle in
596 which both aerobic and anaerobic internal loading will continue to fuel intense algal blooms.
597
598 *Scaling fluxes to the whole ecosystem*
599 A hot spot-hot moment is defined as having a disproportionate influence on elemental
600 cycles at the ecosystem-scale (McClain et al. 2003). As such, we scaled measured P flux rates to
601 representative areas of the lakebed to estimate P loads and determine how the fluxes we
602 classified as hot spots-hot moments actually influenced reservoir-wide internal loading. Hot
603 spots and hot moments of P release from the shallow and intermediate depth sites in late summer
604 under oxic conditions produced the greatest total sediment P load to the reservoir over the study
605 period. This substantial P load resulted from both the high flux rates and the broad spatial extent
606 of sediments releasing P at this time. The importance of littoral areas in governing total internal
607 P loads has also been observed in other waterbodies (Tammeorg et al. 2017). High rates of P
608 release from the deep site in winter and mid-summer did not result in large total P loads due to
609 the small area of lakebed represented by the deep site as well as sediment P retention at other
610 sampling sites. The scaling results further illustrate how even low rates of P release can result in

elevated total P loads if sustained over the entire lakebed. Specifically, we found that low rates of P release across all sampling sites in spring resulted in a high total P load.

Focusing on rates alone may not be sufficient to understand how extreme values of biogeochemical fluxes actually effect ecosystem structure and function. It is essential to scale measurements to the whole system. At the same time, scaling measurements from a single sampling station to an area of the lakebed is fraught with uncertainty. However, we took a conservative approach in assigning representative areas of the lakebed. We also took care in accurately describing the reservoir basin geometry and calculating sediment surface area. As such, we have produced conservative estimates of sediment P loads that can be used to evaluate the ecosystem effects of spatiotemporal variation in P fluxes. Other studies have scaled discrete measurements of sediment P fluxes to larger areas of the lakebed, generally based on waterbody surface area (Scicluna et al. 2015; Noffke et al. 2016). Our approach to characterizing basin geometry allows for more accurate estimates of sediment surface area and thus scaling at finer spatial resolutions based on water depth.

Conclusions

Hot spots and hot moments of sediment P release in the study reservoir arose from interactions between the composition of the sediment P pool and external drivers that determined dissolved oxygen conditions at the sediment-water interface. Our findings demonstrate that the magnitude and mechanisms of internal P loading cannot be understood without capturing both seasonal and spatial variation in fluxes as well as the composition of the sediment P pool as a slow variable. Our understanding of internal P loading in the reservoir would have been very different had we only sampled at one site or in one season. Additionally, scaling flux rates across

the lakebed to estimate internal load revealed that even low rates of P release can result in elevated total P loads if sustained over the entire lakebed. Conversely, very high P flux rates do not necessary produce high total P loads if these fluxes occur over a small area or are balanced by P retention in other regions of the lakebed. These findings illustrate how focusing solely on flux rates without scaling to the whole ecosystem could lead to the misidentification of the main sources and mechanisms of internal loading and ultimately hamper eutrophication management.

Acknowledgements

This research was supported by the Iowa Water Center's Graduate Student Supplemental Research Competition. Albright was supported by the National Science Foundation Graduate Research Fellowship Program under Grant No. DGE-1747503 and 1744592. Any opinions, findings, and conclusions or recommendations expressed in this material are those of the authors and do not necessarily reflect the views of the National Science Foundation. Support was also provided by the Graduate School and the Office of the Vice Chancellor for Research and Graduate Education at the University of Wisconsin-Madison with funding from the Wisconsin Alumni Research Foundation. Wilkinson was supported by the National Science Foundation Division of Environmental Biology grant #1942256 and #2200391.

Literature cited

1. Albright, E.A. 2022. “Spatiotemporal variation in internal phosphorus loading, sediment characteristics, water column chemistry, and thermal mixing in a hypereutrophic reservoir in southwest Iowa, USA (2019-2020).” AlbrightE/GVL_Internal_P_Cycling-Release-2022 Ver. 1. Zenodo. https://doi.org/10.5281/zenodo.6604143
2. Albright, E.A., and G.M. Wilkinson. 2021. Spatiotemporal variation in internal phosphorus loading, sediment characteristics, water column chemistry, and thermal mixing in a hypereutrophic reservoir in southwest Iowa, USA (2019-2020) ver 1. Environmental Data Initiative. https://doi.org/10.6073/pasta/d3a70c1f0d534cca8bdebd7f7483ef38 (Accessed 2021-10-14).
3. Baines, S.B., and M.L. Pace. 1994. Relationships between suspended particulate matter and sinking flux along a trophic gradient and implications for the fate of planktonic primary production. *Canadian Journal of Fisheries and Aquatic Science* **51**:25-36.
4. Bernhardt, E.S., J.R. Blaszczak, C.D. Ficken, M.L. Fork, K.E. Kaiser, and E.C. Seybold. 2017. Control points in ecosystems: Moving beyond the hot spot hot moment concept. *Ecosystems* **20**:665–82.
5. Bivand, R., J. Nowosad, and R. Lovelace. 2021. spData: Datasets for Spatial Analysis. R package version 0.3.10.
6. Buelo, C.D., S.R. Carpenter, and M.L. Pace. 2018. A modeling analysis of spatial statistical indicators of thresholds for algal blooms. *Limnology and Oceanography Letters* **3**:384–392.

7. Caraco, N.F., J.J. Cole, and G.E. Likens. 1993. Sulfate control of phosphorus availability in lakes: A test and re-evaluation of Hasler and Einsele's Model. *Hydrobiologia* **253**: 275-280.
8. Cardoso-Silva, S., P.A.d. Ferreira, R.C.L. Figueira, D.C. Silva, V. Moschini-Carlos, and M.L.M. Pompêo. 2018. Factors that control the spatial and temporal distributions of phosphorus, nitrogen, and carbon in the sediments of a tropical reservoir. *Environmental Science and Pollution Research* **25**:31776–31789.
9. Carpenter, S.R. 2003. Regime Shifts in Lake Ecosystems: Pattern and Variation. Oldendorf/Luhe, Germany: Ecology Institute.
10. Carpenter, S.R., and M.G. Turner. 2000. Hares and tortoises: Interactions of fast and slow variables in ecosystems. *Ecosystems* **3**:495-497.
11. Cavaliere, E., and H.M. Baulch. 2020. Winter in two phases: Long-term study of a shallow reservoir in winter. *Limnology and Oceanography* **66**:1335-1352.
12. Corfidi, S.F., M.C. Coniglio, A.E. Cohen, and C.M. Mead. 2016. A Proposed Revision to the Definition of "Derecho". *Bulletin of the American Meteorological Society* **97**:935-949.
13. Crépin, A. 2007. Using fast and slow processes to manage resources with thresholds. *Environmental & Resource Economics* **36**:191-213.
14. Filzmoser, P., K. Hron, and M. Templ. 2018. Applied Compositional Data Analysis with Worked Examples in R. Spring Series in Statistics. Spring International Publishing, Cham, Switzerland.
15. Forsberg, C. 1989. Importance of sediments in understanding nutrient cyclings in lakes. *Hydrobiologia* **176/177**:263-277.

16. Frost, P.C., C. Prater, A.B. Scott, K. Song, and M.A. Xenopoulos. 2019. Mobility and Bioavailability of Sediment Phosphorus in Urban Stormwater Ponds. *Water Resources Research* **55**:3680-3688.

17. Gakuruh, H. 2017. Essentials of Data Analysis and Graphics Using R. https://helleng.github.io/Data_Mgt_Analysis_and_Graphics_R/Data_Analysis

18. Goff, T.C., M.D. Nelson, G.C. Liknes, T.E. Feeley, S.A. Pugh, and R.S. Morin. 2021. Rapid assessment of tree damage resulting from a 2020 windstorm in Iowa, USA. *Forests* **12**:555.

19. Hayes, N.M., B.R. Deemer, J.R. Corman, N.R. Razavi, and K.E. Strock. 2017. Key differences between lakes and reservoirs modify climate signals: A case for a new conceptual model. *Limnology and Oceanography Letters* **2**:47-62.

20. Horppila, J., H. Holmroos, J. Niemistö, I. Massa, N. Nygrén, P. Schönach, P. Tapio, and O. Tammeorg. 2017. Variations of internal phosphorus loading and water quality in a hypertrophic lake during 40 years of different management efforts. *Ecological Engineering* **103**:264-274.

21. Hudson, J.J., and D.M. Vandergucht. 2015. Spatial and temporal patterns in physical properties and dissolved oxygen in Lake Diefenbaker, a large reservoir on the Canadian Prairies. *Journal of Great Lakes Research* **41**:22-33.

22. Hupfer, M., and J. Lewandowski. 2008. Oxygen controls the phosphorus release from lake sediments – a long-lasting paradigm in limnology. *International Review of Hydrobiology* **93**:415-432.

715 23. Jensen, H.S., and F.Ø. Andersen. 1992. Importance of temperature, nitrate, and pH for
716 phosphate release from aerobic sediments of four shallow, eutrophic lakes. *Limnology*
717 *and Oceanography* **37**:577-598.
718 24. Joshi, S.R., R.K. Kukkadapu, D.J. Burdige, M.E. Bowden, D.L. Sparks, and D.P. Jaisi. 2015.
719 Organic matter remineralization predominates phosphorous cycling in the mid-bay
720 sediments in the Chesapeake Bay. *Environmental Science and Technology* **49**:5887-5896.
721 25. Kimmel, B.L., and A.W. Groeger. 1984. Factors controlling primary production in lakes and
722 reservoirs: A perspective. *Lake and Reservoir Management* **1**:277-281.
723 26. Kleeberg, A., A. Freidank, and K. Jöhnk. 2013. Effects of ice cover on sediment
724 resuspension and phosphorus entrainment in shallow lakes: Combining in situ
725 experiments and wind-wave modeling. *Limnology and Oceanography* **58**:1819-1833.
726 27. Kowalczewska-Madura, K., R. Gołdyn, J. Bogucka, and K. Strzelczyk. 2019. Impact of
727 environmental variables on spatial and seasonal internal phosphorus loading in a
728 mesoeutrophic lake. *International Journal of Sediment Research* **34**:14–26.
729 28. Lukkari, K., H. Hartikainen, and M. Leivuori. 2007. Fractionation of sediment phosphorus
730 revisited. I: Fractionation steps and their biogeochemical basis. *Limnology and*
731 *Oceanography: Methods* **5**:433-444.
732 29. McCarty, J.A. 2019. Sediment phosphorus release in a shallow eutrophic reservoir cove.
733 *Transactions of the ASABE* **62**:1269-1281.
734 30. McClain, M.E., et al. 2003. Biogeochemical hot spots and hot moments at the interface of
735 terrestrial and aquatic ecosystems. *Ecosystems* **6**:301-312.
736 31. Mortimer, C. 1941. The exchange of dissolved substances between mud and water in lakes.
737 *Journal of Ecology* **29**:280-239.

738 32. Murphy, J., and J.P. Riley. 1962. A modified single solution method for the determination of
739 phosphate in natural waters. *Analytica Chimica Acta* **27**:31-36.
740 33. North, R.L., J. Johansson, D.M. Vandergucht, L.E. Doig, K. Liber, K. Lindenschmidt, H.
741 Baulch, and J.J. Hudson. 2015. Evidence for internal phosphorus loading in a large
742 prairie reservoir (Lake Diefenbaker, Saskatchewan). *Journal of Great Lakes Research*
743 **41**:91-99.
744 34. Nowlin, W.H., J.L. Evarts, and M.J. Vanni. 2005. Release rates and potential fates of
745 nitrogen and phosphorus from sediments in a eutrophic reservoir. *Freshwater Biology*
746 **50**:301–322.
747 35. Ogdahl, M.E., A.D. Steinman, and M.E. Weinert. 2014. Laboratory-determined phosphorus
748 flux from lake sediments as a measure of internal phosphorus loading. *Journal of*
749 *Visualized Experiments* **85**:e51617.
750 36. Oksanen, J., et al. 2019. vegan: Community Ecology Package. R package version 2.5-6.
751 37. Orihel, D.M., H.M. Baulch, N.J. Casson, R.L. North, C.T. Parsons, D.C.M Seckar, and J.J.
752 Venkiteswaran. 2017. Internal phosphorus loading in Canadian fresh waters: a critical
753 review and data analysis. *Canadian Journal of Fisheries and Aquatic Science* **74**:2005-
754 2029.
755 38. Ortiz, D.A., and G.M. Wilkinson. 2021. Capturing the spatial variability of algal bloom
756 development in a shallow temperate lake. *Freshwater Biology* **66**:2064-2075.
757 39. Pebesma, E. 2018. Simple features for R: Standardized support for spatial vector data. The R
758 Journal 10:439-446.

759 40. Reedyk, S., E.E. Prepas, and P.A. Chambers. 2001. Effects of single $Ca(OH)_2$ doses on
760 phosphorus concentration and macrophyte biomass of two boreal eutrophic lakes over 2
761 years. *Freshwater Biology* **46**:1075-1087.
762 41. R Core Team. 2019. R: A language and environment for statistical computing. R Foundation
763 for Statistical Computing, Vienna, Austria. https://www.R-project.org/
764 42. Song, K., and A.J. Burgin. 2017. Perpetual phosphorus cycling: Eutrophication amplifies
765 biological control on internal phosphorus loading in agricultural reservoirs. *Ecosystems*
766 **20**:1483-1493.
767 43. Standard Methods for the Examination of Water and Wastewater. 1998. 20th Edition.
768 Method 4500-P B.5.
769 44. Standard Methods for the Examination of Water and Wastewater. 1998. 20th Edition.
770 Method 4500-P E.
771 45. Søndergaard, M., J.P. Jensen, and E. Jeppesen. 2003. Role of sediment and internal loading
772 of phosphorus in shallow lakes. *Hydrobiologia* **506-509**:135-145.
773 46. Tammeorg, O., J. Horppila, P. Tammeorg, M. Haldna, and J. Niemistö. 2016. Internal
774 phosphorus loading across a cascade of three eutrophic basins: A synthesis of short- and
775 long-term studies. *Science of the Total Environment* **572**:943-954.
776 47. Tammeorg, O., T. Möls, J. Niemistö, H. Holmroos, and J. Horppila. 2017. The actual role of
777 oxygen deficit in the linkage of the water quality and benthic phosphorus release:
778 potential implications for lake restoration. *Science of the Total Environment* **599**: 732-
779 738.

48. Tammeorg, O., G. Nürnberg, J. Niemistö, M. Haldna, and J. Horppila. 2020. Internal phosphorus loading due to sediment anoxia in shallow areas: implications for lake aeration treatments. *Aquatic Science* **82**:54.

49. Walker, B.H., S.R. Carpenter, J. Rockstrom, A. Crépin, and G.D. Peterson. 2012. Drivers, "slow" variables, "fast" variables, shocks and resilience. *Ecology and Society* **17**:30.

50. Ward, N.K., et al. 2019. Integrating fast and slow processes is essential for simulating human–freshwater interactions. *Ambio* **48**:1169-1182.

51. Walsh, J.R., J.R. Corman, and S.E. Munoz. 2018. Coupled long-term limnological data and sedimentary records reveal new control on water quality in a eutrophic lake. *Limnology and Oceanography* **64**:S34-S48.

52. Wuertz, D., T. Setz, Y. Chalabi, C. Boudt, P. Chausse, and M. Miklovac. 2020. fGarch: Rmetrics - Autoregressive Conditional Heteroskedastic Modelling. R package version 3042.83.2.

Tables

Table 1. Thermal stratification and dissolved oxygen conditions at the sediment-water interface.

DOY	Season	Site	Water Column Thermal Structure	Bottom Water Temperature (°C)	Bottom Water DO (mg L^{-1})	Bottom Water DO Saturation (%)
39	Winter	Intermediate	Stratified	3.2	12.6	94.3
		Deep	Stratified	4.2	1.1	8.6
117	Spring	Shallow	Isothermal	14.6	9.4	92.5
		Intermediate	Stratified	14.1	8.9	86.4
		Deep	Stratified	11.9	5.8	54.3
181	Mid-Summer	Shallow	Isothermal	26.5	5.4	67.4
		Intermediate	Isothermal	26.3	6.3	78.0
		Deep	Isothermal	24.2	0.3	3.3
223	Late Summer	Shallow	Isothermal	26.1	7.2	88.7
		Intermediate	Isothermal	25.4	4.8	58.0
		Deep	Isothermal	24.9	4.5	54.2
298	Autumn	Shallow	Isothermal	6.7	10.2	83.3
		Intermediate	Isothermal	8.1	8.7	73.7
		Deep	Isothermal	8.4	8.7	73.8

Figure legends

Figure 1. Sampling sites in Green Valley Lake, Iowa, USA. The three sampling sites are representative of different areas of the lakebed based on water depth. The shaded polygons illustrate these areas. The shallow site is representative of the 1.2-3.6 m depth contour. The intermediate depth site is representative of the 3.6-5.6 m interval, and the deep site is representative of the area deeper than 5.6 m.

Figure 2. Sediment P flux rates and bottom water P concentrations. (Top row of panels) Time series of mean sediment total P flux (± standard error among three replicate cores) from February to October of 2020. The shallow site was not sampled in February due to unsafe ice conditions. Negative values indicate sediment P retention while positive values show P release. (Bottom row of panels) Time series of bottom water total P (TP) and soluble reactive P (SRP) concentrations for each sampling site over the study period.

Figure 3. Mean sediment P flux rates (± standard error among three replicate cores) across the range of observed bottom water dissolved oxygen (DO) concentrations.

Figure 4. Spatiotemporal variation in sediment P species. (A) Average, annual sediment P composition by sampling site. Refractory P is estimated as the difference between total P and the sum of the measured P fractions. The relative abundance of each P species as a percent of the total sediment P pool is noted. Time series of mean (± standard error of three replicate samples) (B) redox-sensitive, (C) labile organic, (D) aluminum-bound, and (E) loosely-bound P

concentrations across sampling sites and over the course of the year. Note different y-axis scales across plots depicting more versus less abundant P fractions.

Figure 5. Spatiotemporal variation in sediment P composition. PCA biplot based on a compositional data analysis of sediment P pools over the course of the year and across the reservoir.

Figure 6. Estimated mean P load at the time of sampling by site (bars) and total load across the lakebed (points; error bars are ± standard error). Bar plots show the mean, estimated P load for each sampling site at the time of sampling. Points represent the sum of the estimated loads across the lakebed.

Figures

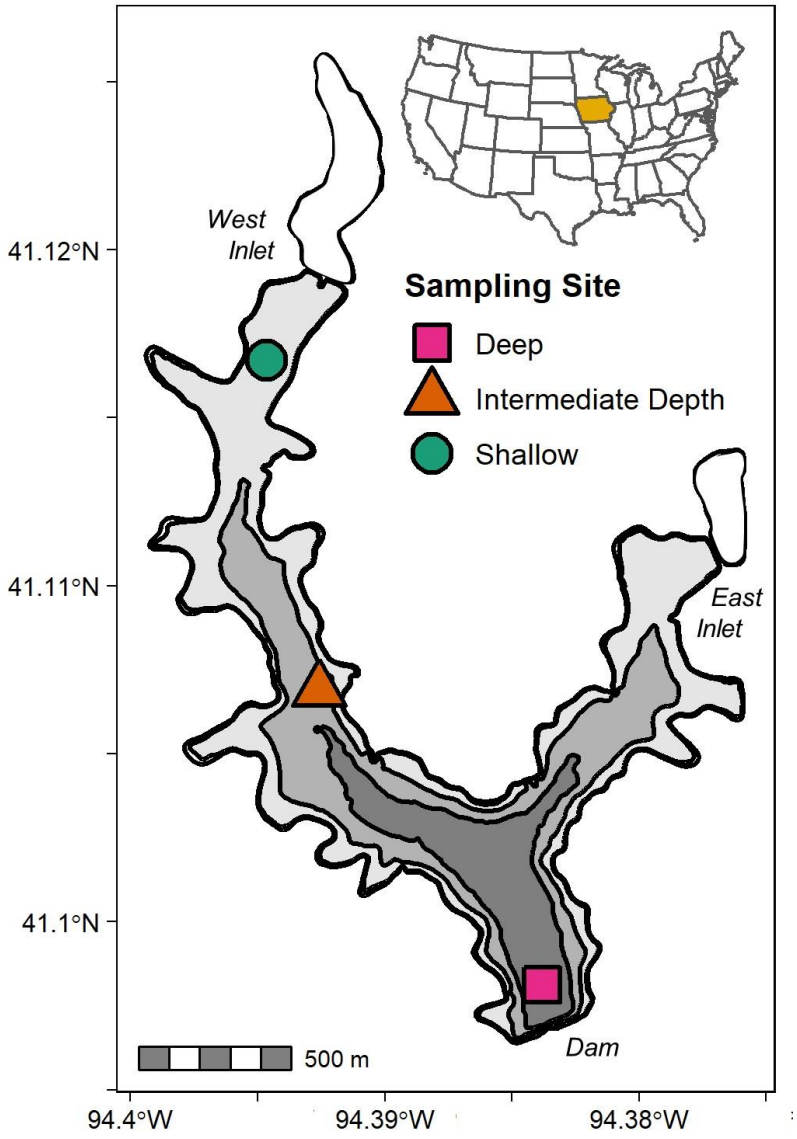

Figure 1. Sampling sites in Green Valley Lake, Iowa, USA. The three sampling sites are representative of different areas of the lakebed based on water depth. The shaded polygons illustrate these areas. The shallow site is representative of the 1.2-3.6 m depth contour. The intermediate depth site is representative of the 3.6-5.6 m interval, and the deep site is representative of the area deeper than 5.6 m.

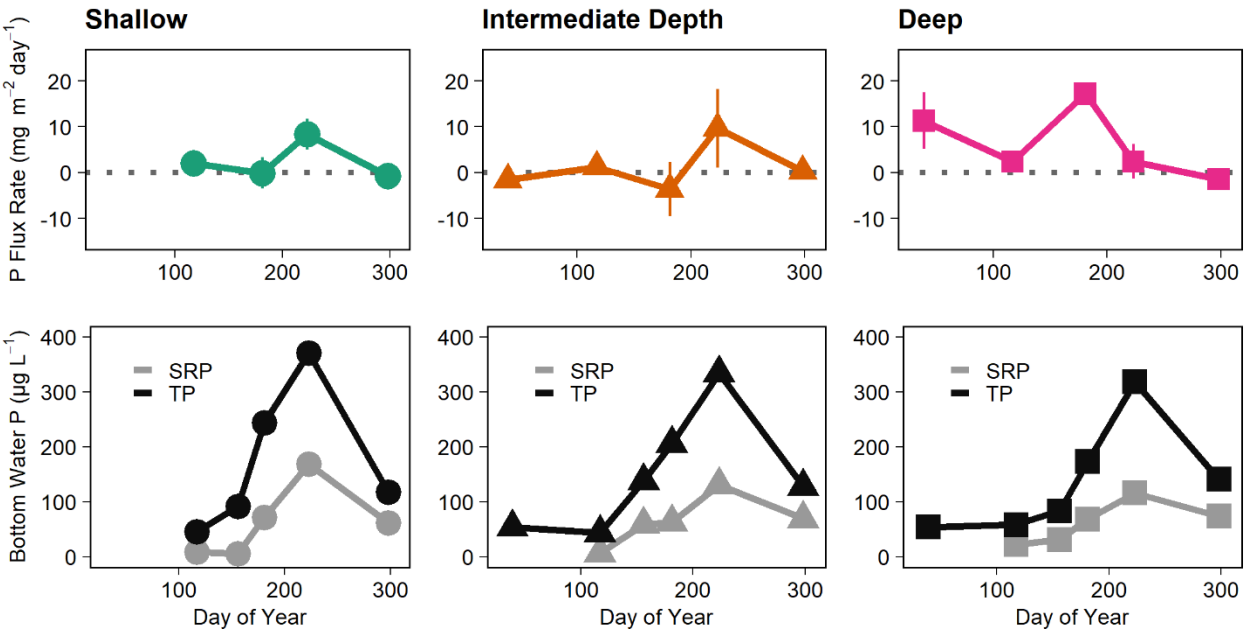

839

840 **Figure 2.** Sediment P flux rates and bottom water P concentrations. (Top row of panels) Time
841 series of mean sediment total P flux (± standard error among three replicate cores) from February
842 to October of 2020. The shallow site was not sampled in February due to unsafe ice conditions.
843 Negative values indicate sediment P retention while positive values show P release. (Bottom row
844 of panels) Time series of bottom water total P (TP) and soluble reactive P (SRP) concentrations
845 for each sampling site over the study period.

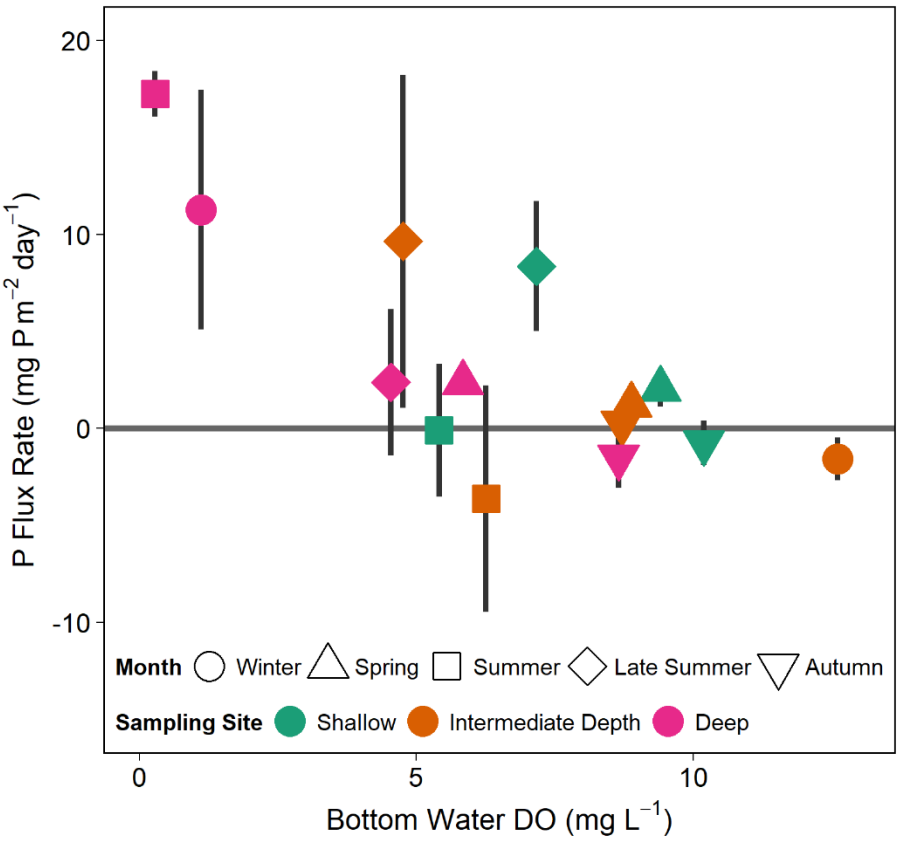

846

847 **Figure 3.** Mean sediment P flux rates (± standard error among three replicate cores) across the

848 range of observed bottom water dissolved oxygen (DO) concentrations.

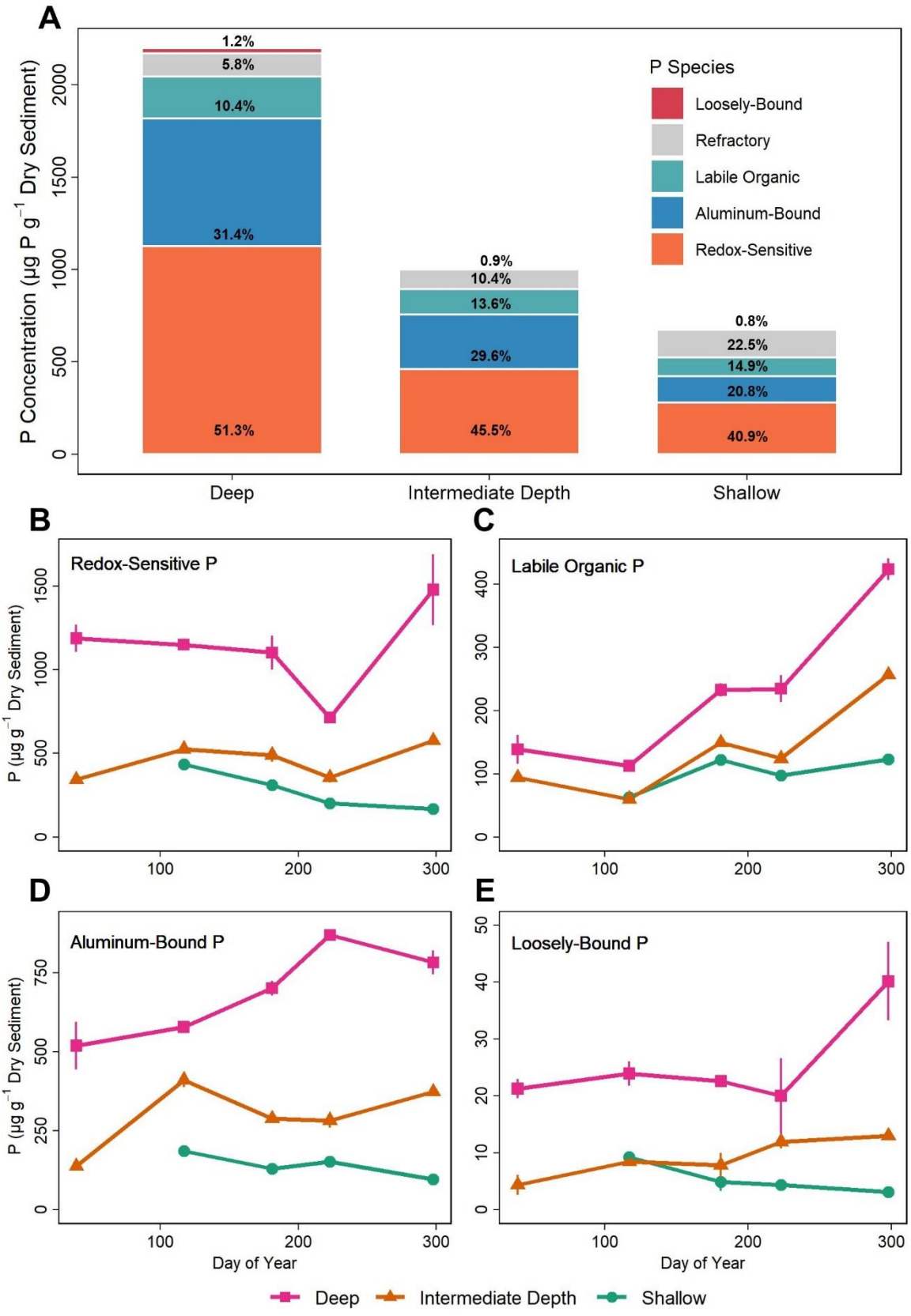
A
P Concentration (µg P g^{-1} Dry Sediment)
0
500
1000
1500
2000
1.2%
5.8%
10.4%
31.4%
51.3%
0.9%
10.4%
13.6%
29.6%
45.5%
0.8%
22.5%
14.9%
20.8%
40.9%
P Species
Loosely-Bound
Refractory
Labile Organic
Aluminum-Bound
Redox-Sensitive
Deep
Intermediate Depth
Shallow
B
Redox-Sensitive P
C
Labile Organic P
D
Aluminum-Bound P
E
Loosely-Bound P
P (µg g^{-1} Dry Sediment)
Day of Year
100
200
300
Deep
Intermediate Depth
Shallow

849

Figure 4. Spatiotemporal variation in sediment P species. (A) Average, annual sediment P composition by sampling site. Refractory P is estimated as the difference between total P and the sum of the measured P fractions. The relative abundance of each P species as a percent of the total sediment P pool is noted. Time series of mean (± standard error of three replicate samples) (B) redox-sensitive, (C) labile organic, (D) aluminum-bound, and (E) loosely-bound P concentrations across sampling sites and over the course of the year. Note different y-axis scales across plots depicting more versus less abundant P fractions.

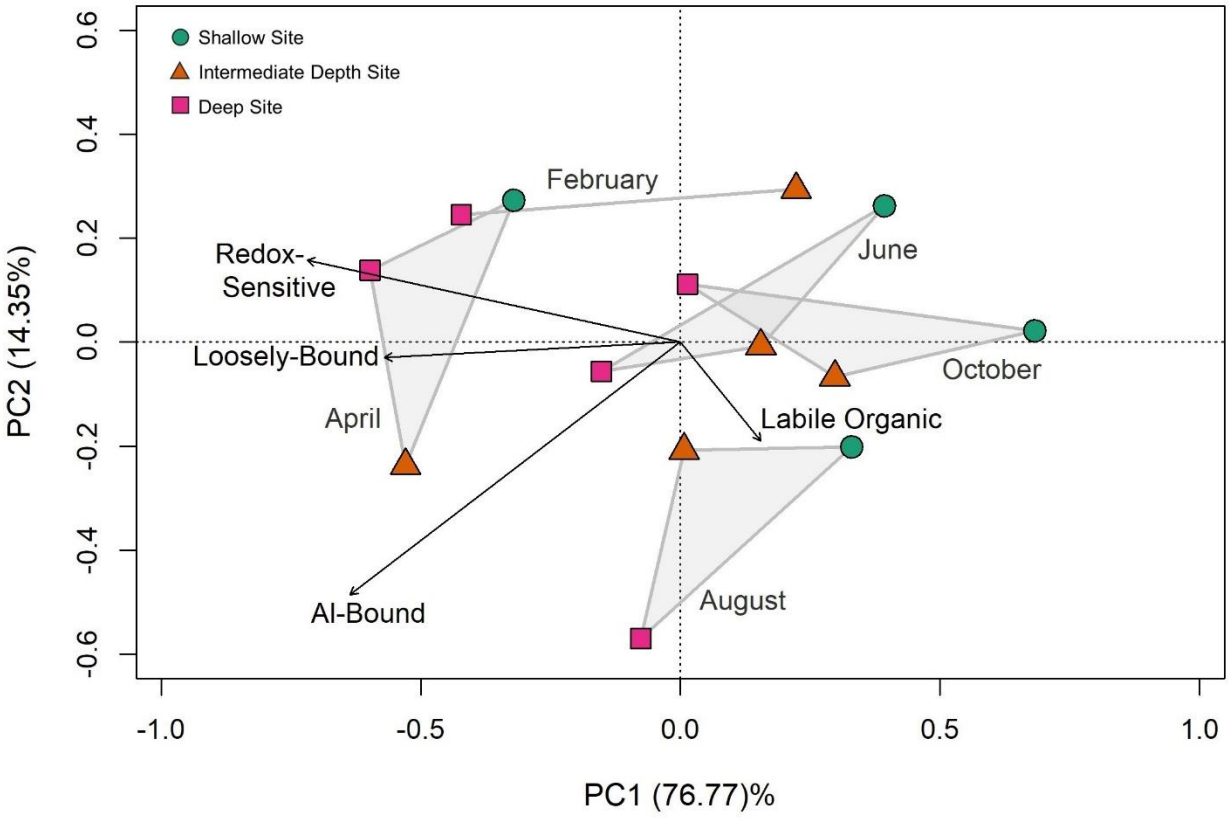

Figure 5. Spatiotemporal variation in sediment P composition. PCA biplot based on a compositional data analysis of sediment P pools over the course of the year and across the reservoir.

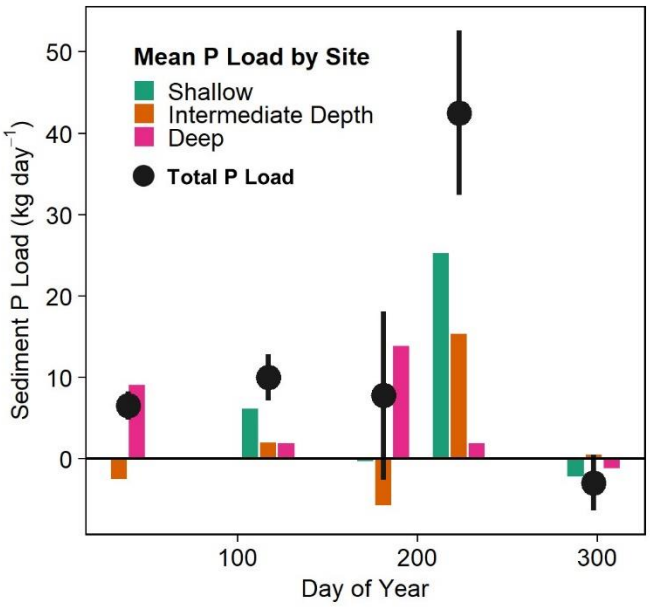

Figure 6. Estimated mean P load at the time of sampling by site (bars) and total load across the lakebed (points; error bars are ± standard error). Bar plots show the mean, estimated P load for each sampling site at the time of sampling. Points represent the sum of the estimated loads across the lakebed.

Appendix S1 - Ecosphere

Sediment phosphorus composition controls hot spots and hot moments of internal loading in a temperate reservoir

Ellen A. Albright[1,2†] and Grace M. Wilkinson[1,2]

[1]Dept. of Ecology, Evolution and Organismal Biology, Iowa State University, Ames, IA, USA

[2]Center for Limnology, University of Wisconsin-Madison, Madison, WI, USA

[†] Corresponding Author: ealbright2@wisc.edu

Introduction

The appendix contains additional methods text detailing analysis of suspended solids, total nitrogen, and nitrate as well as use of previous monitoring data. We provide the equations used to determine sediment phosphorus (P) flux rates as well as sediment physical characteristics and the concentrations of sediment total P and various P species. We have also provided the standard equation for the third statistical moment. Table S1 compares temperature and dissolved oxygen conditions between the core incubations and ambient conditions in the reservoir for each sampling site and event. Table S2 details surface and bottom water chemistry including total, volatile, and involatile suspended solids; total and soluble reactive P; total nitrogen; and nitrate concentrations. Table S2 reports the mean P flux rates by site and event, as presented in Figure 2 in the manuscript. Table S4 demonstrates the effects of excluding high flux rates on the skewness of the P flux distribution, as quantified by the third statistical moment. Table S5 provides loss on ignition organic matter, moisture content, and bulk density data. Table S6 reports the estimated mean sediment P load by site and sampling event as well as the estimated total internal load.

Figure S1 plots temperature and dissolved oxygen conditions in the incubating cores against ambient conditions in the reservoir for each sampling site and event. We included a visualization that compares 2020 epi- and hypolimnetic total P and soluble reactive P concentrations to the P dynamics from previous years (Figure S2). Figure S3 illustrates the distribution of sediment P flux rates across sampling sites and seasons, with statistical outliers noted. Figure S4 breaks down the sediment P flux rate data by site and sampling event to identify the points in space and time associated with high flux rates. Figure S5 displays the time series of sediment total P by sampling site. We include citations for all references included in the appendix as well as citations for additional R packages used solely for data cleaning and visualizations.

Vertical profiles and water chemistry

Suspended solids

Total suspended solids were determined by filtering a known volume of sample water through a prepared filter (0.45µm GF/C filters) and drying to a constant weight. Volatile suspended solids were determined via loss-on-ignition, and involatile solids were assumed to be the difference between volatile and total suspended solids.

Total nitrogen and nitrate

Subsamples were filtered (0.45µm GF/C filters) in the lab for nitrate analysis, and all samples were preserved with concentrated sulfuric acid to pH 2. Total nitrogen samples underwent digestion prior to analysis (Standard Methods 4500-N.C). Total nitrogen and nitrate were measured via second-derivative ultraviolet spectroscopy (Crumpton and others 1992, Childress and others 1999) using an HP 8453 Spectrophotometer.

Use of previous monitoring data

In order to compare water column nutrient dynamics in 2020 to previous years, we used publicly-available nutrient monitoring data from the Iowa Department of Natural Resources AQuIA database (Figure S1).

Sediment P fluxes

Equation S1 – *Mass of P in the Overlying Water*

$$\text{Water Column Mass P (mg)} = \text{Water column [TP] (mg/L)} * (\text{Total Water Volume (L)} - \text{Replacement Water Volume (L)}) \quad (1)$$

Equation S2 – *Mass of P in the Replacement Water*

$$\text{Replacement Water Mass P (mg)} = \text{Replacement Water [TP] (mg/L)} * \text{Replacement Water Volume (L)} \quad (2)$$

Equation S3 – *New TP Concentration Following Addition of Replacement Water*

$$\text{New [TP] (mg/L)} = (\text{Water Column Mass P (mg)} + \text{Replacement Water Mass P (mg)}) / \text{Total Water Volume (L)} \quad (3)$$

Equation S4 – *Daily Change in TP Concentration*

$$\Delta\,[\text{TP}]\ (\text{mg/L}) = \text{Water Column } [\text{TP}]_{\text{day n}}\ (\text{mg/L}) - \text{New } [\text{TP}]_{\text{day n-1}}\ (\text{mg/L}) \quad (4)$$

Sediment P content and composition

Additional subsamples of fresh sediment were used for analysis of physical characteristics. For each site, three replicate subsamples were dried to a constant mass and the wet and dry masses were used to determine sediment moisture content (MC). The subsamples were then combusted and weighed again to calculate organic matter content as loss-on-ignition (LOI) and estimate bulk density (Håkanson and Jansson 2002).

Equation S5 – *Moisture Content (MC)*

$$\text{Moisture Content (\%)} = \left[\frac{(W_w - W_t) - (W_d - W_t)}{W_w - W_t}\right] \times 100 \quad (5)$$

Where W_t is the weight of the aluminum weigh boat, W_w is the weight of the weigh boat and fresh sediment sample, and W_d is the weight of the weigh boat and dry sediment.

Equation S6 – *Organic Matter Content as Loss-on-Ignition (LOI)*

$$\text{LOI Organic Matter Content (\%)} = \left[\frac{(W_d - W_t) - (W_a - W_t)}{W_d - W_t}\right] \times 100 \quad (6)$$

Where W_a is the weight of the weigh boat and the ashed sediment after combustion.

Equation S7 – *Bulk Density*

$$\text{Bulk Density } \left(g/cm^3\right) = \frac{260}{100 + 1.6 \times \left[MC + \left(\frac{LOI}{100 \times (100 - MC)}\right)\right]} \quad (7)$$

Equation S8 – *Dry Mass Equivalent of Fresh Sediment Used*

$$\text{Dry Mass Equivalent (g)} = \text{Mass Fresh Sediment (g)} \times (100 - MC) \quad (8)$$

Equation S9 – *Loosely-Sorbed and Pore Water P*

$$\text{Loosely-Bound P (mg P/g dry sediment)} = \frac{\text{Concentration TP (mg/L)} \times \text{Solution Volume (L)}}{\text{Dry Mass Equivalent of Sediment Used (g)}} \quad (9)$$

The concentration of TP used should reflect the average of lab duplicates, corrected for any dilutions. The solution volume should equal the total amount of 0.46 M NaCl extractant and rinse solutions (0.1 L total). The dry mass equivalent of the fresh sediment used is estimated based on MC (Eq. 4) and will be the same for the calculations of each subsequent extraction.

Equation S10 – *Redox-Sensitive P*

$$\text{Redox-Sensitive P (mg P/g dry sediment)} = \frac{\text{Concentration TP (mg/L)} \times \text{Solution Volume (L)}}{\text{Dry Mass Equivalent of Sediment Used (g)}} \quad (10)$$

The concentration of TP used should reflect the average of lab duplicates, corrected for any dilutions. The solution volume should equal the total volume of the 0.11 M bicarbonate – 0.1 M sodium dithionate solution and the rinse solutions (0.2 L total).

Equation S11 – *Aluminum-Bound P*

$$\text{Al-Bound P (mg P/g dry sediment)} = \frac{\text{Concentration SRP (mg/L)} \times \text{Solution Volume (L)}}{\text{Dry Mass Equivalent of Sediment Used (g)}} \quad (11)$$

The concentration of SRP used should reflect the average of lab duplicates, corrected for any dilutions. The solution volume should equal the total volume of 0.1 M NaOH used and the rinse solutions (0.150 L total).

Equation S12 – *Labile Organic P*

$$\text{Labile Organic P (mg P/g dry sediment)} = \left[\frac{\text{Concentration TP (mg/L)} \times \text{Solution Volume (L)}}{\text{Dry Mass Equivalent of Sediment Used (g)}}\right] - \text{Al-Bound P} \quad (12)$$

The concentration of TP from the supernatant should first be corrected for the volume of NaOH and rinse solutions used (0.15 L total) and the sediment mass. This value represents the concentration of aluminum-bound and total labile organic P in the sediment pellet. The concentration of labile organic P is calculated as the difference between this value and the Al-bound P concentration (Eq. 7).

Equation S13 – *Total P*

$$\text{Total P (mg P/g dry sediment)} = \frac{\left[\text{Concentration TP}\left(\frac{\text{mg}}{\text{L}}\right) \times \frac{\text{(Post pH (g)-Tare (g))}}{\text{(Pre pH (g)-Tare (g))}}\right] \times \text{Dilution Volume (L)}}{\text{Dry Mass of Sediment Used (g)}} \quad (13)$$

The concentration of TP used should reflect the average of lab duplicate measures and must be corrected for the pH adjustment. The corrected TP concentration can then be corrected for the volume to which the sample was diluted after boiling (0.05 L) and the mass of dry sediment.

Statistical Analyses

Equation S14 – *Skewness, third statistical moment (m_3)*

$$m_3 = \frac{\sum(x-\mu)^3}{n} \quad (14)$$

The third statistical moment quantifies skewness and can be standardized by dividing by the cube of the standard deviation. Perfectly symmetric distributions have an m3 value of zero.

978 **Table S1.** Incubation versus reservoir temperature and dissolved oxygen conditions

		Temperature (°C)			Dissolved Oxygen (mg L^{-1})		
Month	Site	Reservoir Bottom Water	Core Mean	Core SEM	Reservoir Bottom Water	Core Mean	Core SEM
February	Intermediate	3.2	6.4	0.1	12.6	12.0	0.1
	Deep	4.2	5.4	0.1	1.1	1.8	0.6
April	Shallow	14.6	11.4	0.2	9.4	10.3	0.1
	Intermediate	14.1	11.1	0.1	8.9	10.2	0.1
	Deep	11.9	11.4	0.2	5.8	7.5	0.4
June	Shallow	26.5	23.0	0.1	5.4	7.3	0.1
	Intermediate	26.3	22.8	0.1	6.3	6.2	0.4
	Deep	24.2	22.8	0.1	0.3	1.4	0.1
August	Shallow	26.1	24.6	0.3	7.2	6.6	0.2
	Intermediate	25.4	24.6	0.3	4.8	1.9	0.1
	Deep	24.9	24.8	0.3	4.5	1.6	0.2
October	Shallow	6.7	10.2	0.2	10.2	10.7	0.1
	Intermediate	8.1	10.4	0.1	8.7	10.3	0.2
	Deep	8.4	11.1	0.3	8.7	10.4	0.1

979

Table S2. Epi- and hypolimnetic water chemistry by site and sampling event

			Suspended Solids (mg L^{-1})			Phosphorus (µg L^{-1})		Nitrogen (mg L^{-1})	
DOY	Site	Water Column	TSS	VSS	ISS	TP	SRP	TN	No_x
39	Intermediate	Surface	NA	NA	NA	49.6	NA	NA	NA
		Bottom	7.5	4.5	3.0	54.2	NA	NA	0.4
	Deep	Surface	NA	NA	NA	42.7	NA	NA	NA
		Bottom	5.5	NA	NA	53.9	NA	NA	0.3
117	Shallow	Surface	1.1	NA	NA	39.5	7.1	1.0	0.7
		Bottom	9.5	NA	NA	45.6	9.3	0.9	0.7
	Intermediate	Surface	12.2	NA	NA	33.7	5.5	0.8	0.6
		Bottom	3.0	NA	NA	43.7	7.3	0.8	0.7
	Deep	Surface	5.5	NA	NA	35.0	1.9	0.6	0.6
		Bottom	1.5	NA	NA	58.5	22.0	0.7	0.4
181	Shallow	Surface	36.7	25.7	11.0	251.2	66.9	1.3	0.1
		Bottom	30.3	18.7	11.7	243.6	71.6	1.0	0.1
	Intermediate	Surface	22.0	17.0	5.0	327.4	63.0	0.9	0.1
		Bottom	22.1	15.3	6.8	206.0	63.3	1.0	0.0
	Deep	Surface	15.0	13.0	2.0	178.7	59.6	0.7	0.1
		Bottom	16.4	14.8	1.7	173.0	68.7	0.9	0.1
223	Shallow	Surface	51.0	28.5	22.5	376.4	173.1	1.3	0.1
		Bottom	43.5	21.0	22.5	370.9	168.5	1.3	0.1
	Intermediate	Surface	41.0	29.5	11.5	343.6	134.0	1.4	0.1
		Bottom	40.0	20.0	20.0	334.0	131.2	1.2	0.1
	Deep	Surface	38.0	19.0	19.0	330.3	116.6	1.1	0.1
		Bottom	32.0	17.5	14.5	318.0	116.3	1.3	0.1
298	Shallow	Surface	6.6	NA	NA	115.9	61.6	1.0	0.3
		Bottom	3.2	NA	NA	118.1	62.3	0.9	0.3
	Intermediate	Surface	8.0	NA	NA	131.6	69.2	1.0	0.3
		Bottom	17.6	NA	NA	128.4	69.7	1.0	0.3
	Deep	Surface	6.2	NA	NA	138.4	71.0	1.0	0.2
		Bottom	2.4	NA	NA	141.1	74.3	1.0	0.3

Surface water samples were taken 0.25 m below the surface and bottom water samples were taken 0.5 m above the sediment-water interface. Suspended solid constituents measured include total (TSS), volatile (VSS) and involatile (ISS).

Table S3. Mean P flux rates across sampling sites and seasons.

	Mean P Flux Rate ± Standard Error (mg P m^{-2} day^{-1})				
Sampling Site	***February***	***April***	***June***	***August***	***October***
Shallow		2.0 ± 0.9	-0.1 ± 3.4	8.4 ± 3.4	-0.7 ± 1.1
Middle	-1.6 ± 1.1	1.2 ± 0.2	-3.6 ± 5.8	9.6 ± 8.6	0.3 ± 0.7
Deep	11.3 ± 6.2	2.4 ± 0.3	17.2 ± 1.2	2.4 ± 3.8	-1.5 ± 1.6

Values indicate the mean P flux rate ± standard error across three replicate sediment cores. Blue cells indicate sediment P retention, orange cells corresponded to sediment P release, and either retention or release may have occurred during times indicated in grey.

Table S4. Influence of excluding high flux rates on distribution skewness.

Dataset Subsample	***Standardized Third Statistical Moment (m_3)***	***Distribution Shape***
Full dataset	0.818	Moderately positively skewed
Exclude highest flux	0.734	Moderately positively skewed
Exclude 2 highest fluxes	0.718	Moderately positively skewed
Exclude 3 highest fluxes	0.666	Moderately positively skewed
Exclude 4 highest fluxes	0.584	Moderately positively skewed
Exclude 5 highest fluxes	0.462	approximately symmetric

Table S5. Sediment physical characteristics

		LOI Organic Matter (%)		Moisture Content (%)		Bulk Density (g cm^{-3})	
Site	Month	Mean	SEM	Mean	SEM	Mean	SEM
Shallow	April	9.28	0.42	71.70	0.31	1.19	0.0034
	June	9.37	0.01	71.49	0.18	1.19	0.0014
	August	8.96	0.34	73.24	0.35	1.18	0.0034
	October	7.13	1.95	70.42	1.22	1.20	0.0049
Intermediate	February	7.49	0.29	69.36	0.32	1.21	0.0028
	April	8.54	0.30	78.15	0.58	1.14	0.0048
	June	9.71	0.08	77.12	0.21	1.15	0.0016
	August	9.53	0.36	79.79	0.34	1.13	0.0026
	October	8.42	2.00	82.95	0.67	1.11	0.0021
Deep	February	12.32	0.36	85.25	0.23	1.09	0.0013
	April	14.97	1.28	86.07	0.19	1.08	0.0017
	June	12.73	1.18	86.81	0.31	1.08	0.0010
	August	14.03	0.14	87.21	0.07	1.07	0.0003
	October	11.65	1.43	86.67	0.10	1.08	0.0008

The shallow site was not sampled in February due to unsafe ice conditions. Mean and standard error values represent either three laboratory replicates (February-August) or two replicates (October sampling event).

Table S6. Estimated mean P load by site and total load.

	Lakebed Information		Estimated Mean P Load ± Standard Error (kg P day^{-1})				
Site	Depth Contour	Sediment Area (m^2)	Winter	Spring	Mid-Summer	Late Summer	Autumn
Shallow	1.2-3.6 m	3,014,983.6	n.a.	6.2 ± 2.8	-0.3 ± 10.3	25.2 ± 10.1	-2.2 ± 3.4
Intermediate	3.6-5.6 m	1,593,676.1	-2.5 ± 1.7	1.9 ± 0.3	-5.8 ± 9.3	15.4 ± 13.7	0.4 ± 1.1
Deep	> 5.6 m	801,995.5	9.0 ± 5.0	1.9 ± 0.2	13.8 ± 0.9	1.9 ± 3.0	-1.2 ± 1.3
Estimated Total Load (kg Pday^{-1})			6.5 ± 1.7	10.0 ± 2.8	7.8 ± 10.3	42.5 ± 10.1	-2.9 ± 3.4

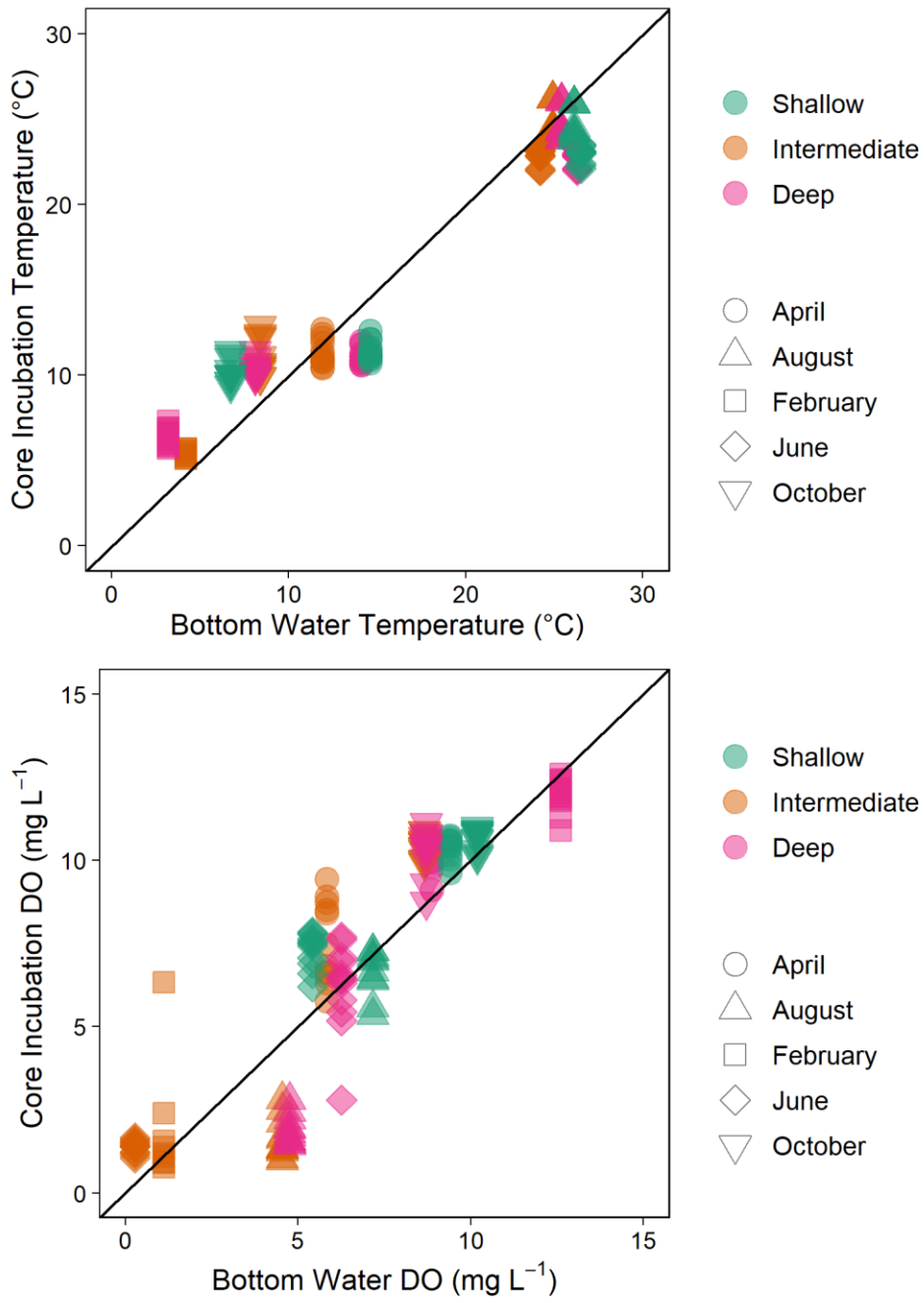

Figure S1. *Comparison of core incubation conditions to reservoir conditions.* The mean temperature (top panel) and dissolved oxygen concentration (bottom panel) across replicate cores are plotted against bottom water conditions at the corresponding sampling sites for each sampling event.

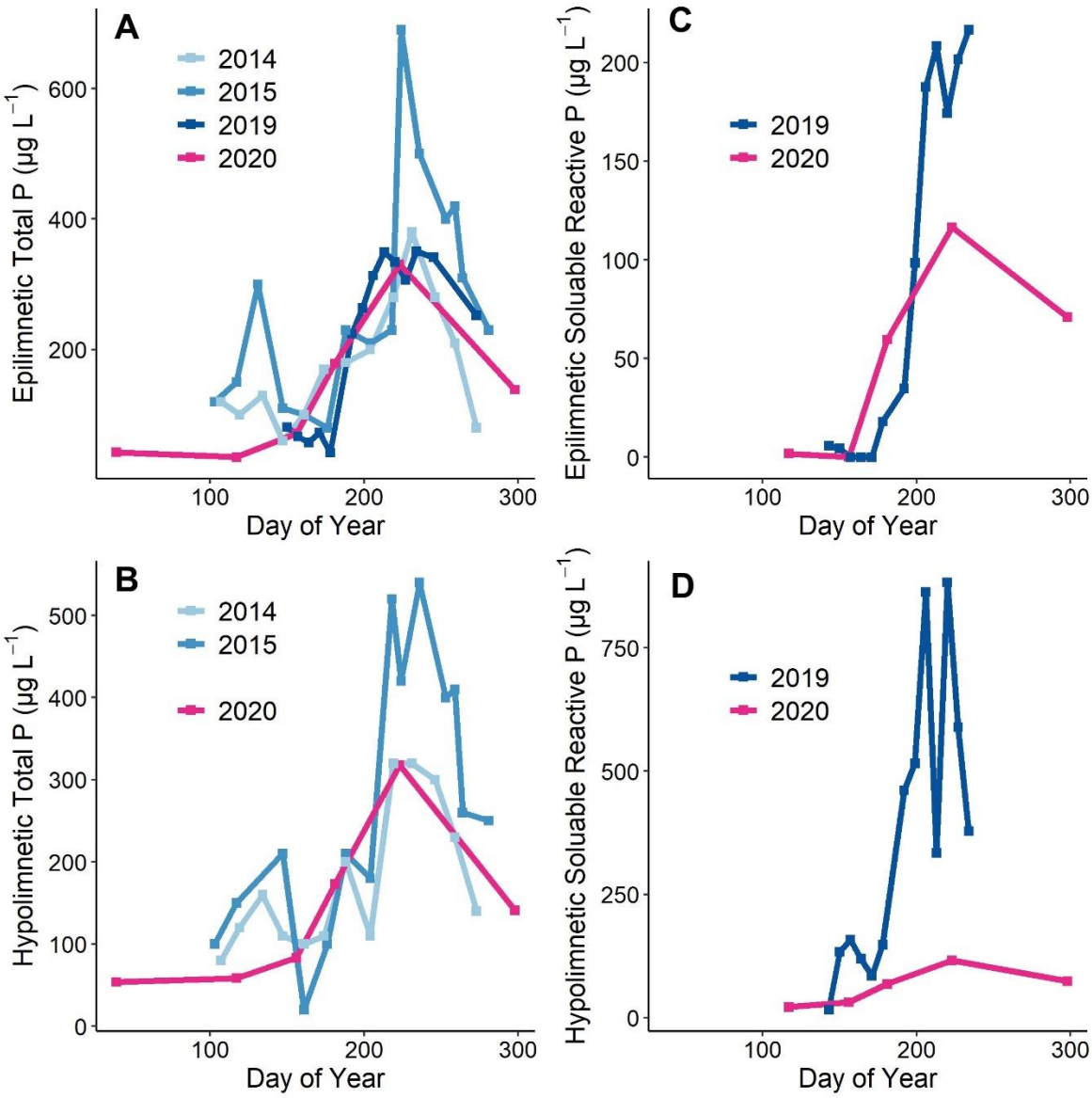

1006

1007 **Figure S2.** *Comparing 2020 epi- and hypolimnetic P dynamics to previous years (2014, 2015,*
1008 *2019).* The 2020 P dynamics followed similar seasonal trends as past years in epilimnetic TP (A)
1009 and hypolimnetic TP (B) concentrations. Epilimnetic and hypolimnetic SRP concentrations were
1010 higher in 2019 than in 2020 (C-D).

1011

1012

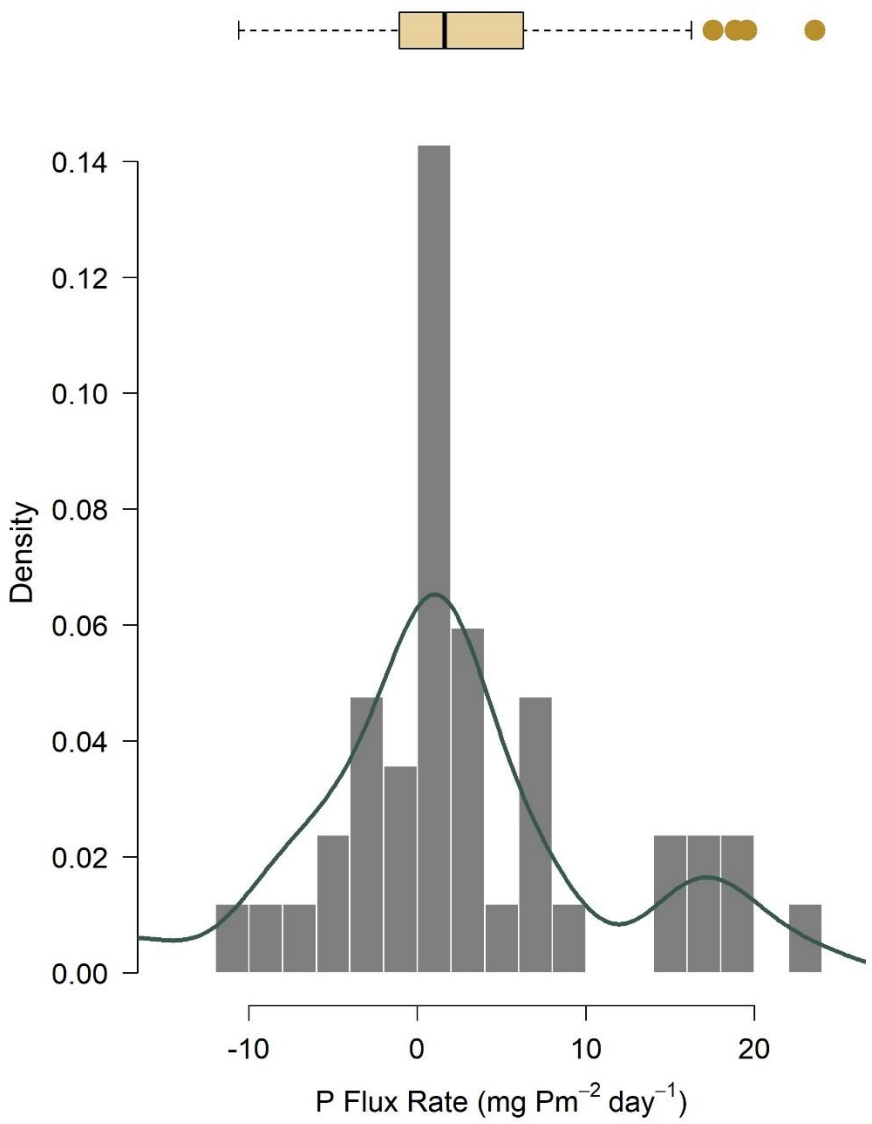

Figure S3. *Distribution of sediment P flux rates.* The histogram details measured sediment P flux rates over all sampling sites and seasons while the density curve provides a kernel density estimation. The distribution and statistical outliers are further summarized with a boxplot.

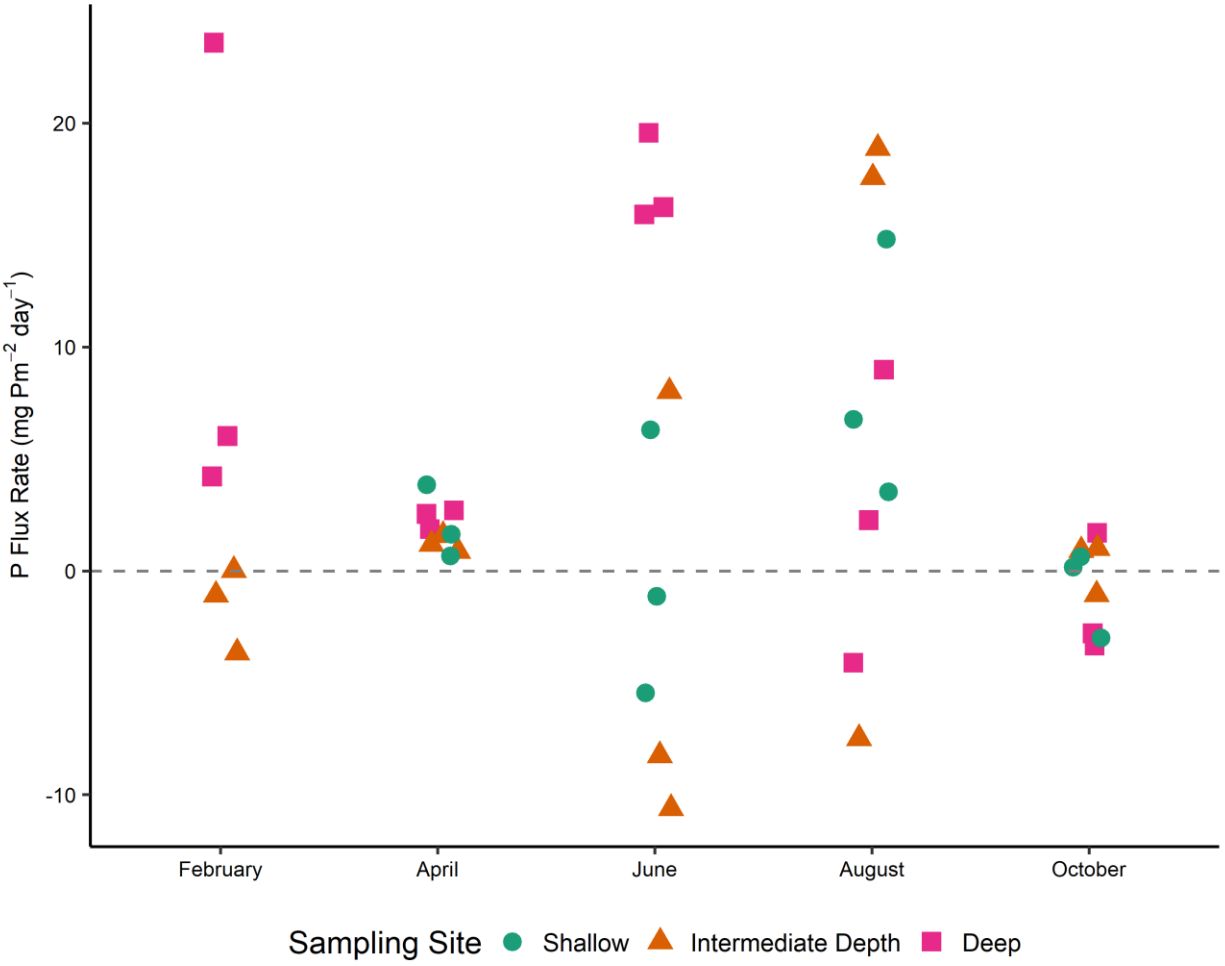

Figure S4. *Sediment P flux rates by site and sampling event, 2020.* The distribution of all measured sediment P flux rates is visualized by sampling site and month. The highest observed release rates were associated with sediments from the deep sampling site in February and June as well as August fluxes from the middle and shallow sites. The four highest rates are statistical outliers.

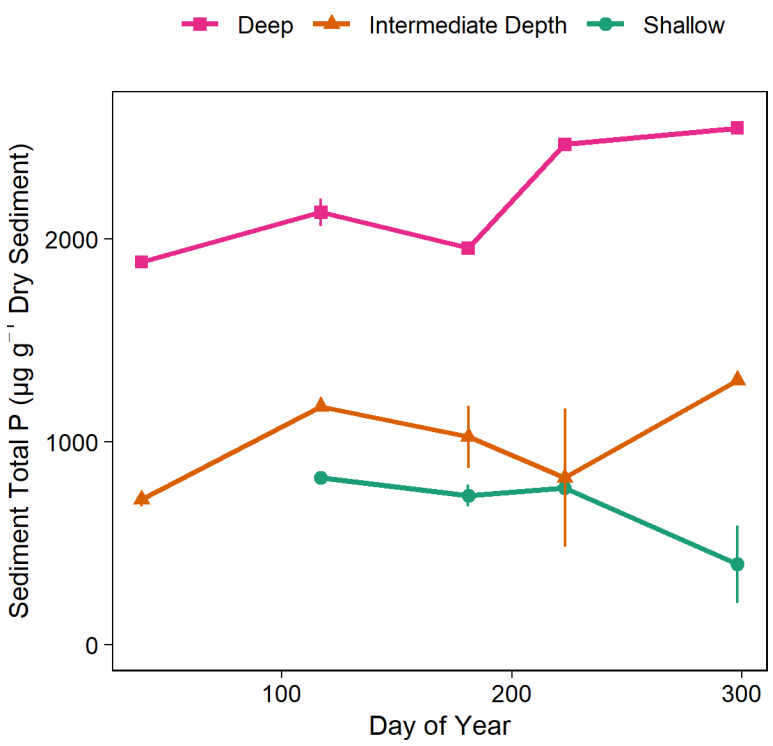

Figure S5. Spatiotemporal variation in sediment total P. Time series of mean total P concentrations over time for each sampling site. Error bars represent one standard error

Appendix literature cited

1. Childress, C.J.O., W.T. Foreman, B.F. Conner, and T.J. Maloney. 1999. New Reporting Procedures Based on Long-Term Method Detection Levels and Some Considerations for Interpretations of Water-Quality Data Provided by the U.S. Geological Survey National Water Quality Laboratory. U.S. Geological Survey Open File Report 99-193. 24 p.
2. Crumpton, W.G., T.M. Isenhart, and P.D. Mitchel. 1992. Nitrate and organic N analyses with second-derivative spectroscopy. Limnology and Oceanography 37:907-913.
3. Håkanson, L., and M. Jansson. 2002. Principles of lake sedimentology. Caldwell, NJ: The Blackburn Press.
4. Standard Methods for the Examination of Water and Wastewater. 1998. 20th Edition. Method 4500-N N.C.

R packages used for data cleaning and visualizations

tidyverse (Wickham and others 2019), RColorBrewer (Neuwirth 2014), gridExtra (Auguie 2017), cowplot (Wilke 2020), ggspatial (Dunnington 2021)

1. Auguie, B.. 2017. gridExtra: Miscellaneous Functions for "Grid" Graphics. R package version 2.3.
2. Dunnington, D. 2021. ggspatial: Spatial Data Framework for ggplot2. R package version 1.1.5.
3. Neuwirth, E. 2014. RColorBrewer: ColorBrewer Palettes. R package version 1.1-2.
4. Wickham, H., et al. 2019. Welcome to the tidyverse. Journal of Open Source Software 4:1686.
5. Wilke, C.O. 2020. cowplot: Streamlined Plot Theme and Plot Annotations for 'ggplot2'. R package version 1.1.1.